

# $R$ measurement and QCD studies at future super $\tau - c$ factory

Guangshun Huang\*, Wenbiao Yan and Xiaorong Zhou  
(On behalf of STCF working group)

University of Science and Technology of China, Hefei 230026, China

## Abstract

We review status of  $R$  measurement and QCD studies at low energy range, discuss prospects for a super  $\tau$ -charm factory in 2 – 7 GeV. With a high-luminosity  $e^+e^-$  collider, statistics are no longer problem for  $R$  measurement and a precision of 2% or even better is foreseen, that will lead to bring down the uncertainty of hadronic contribution to the QED running coupling constant  $\Delta\alpha_{had}$  and the anomalous magnetic moment of the muon ( $a_\mu$ ); measure the strong coupling constant  $\alpha_s$  and the charm quark mass; improve the measurement of the resonance parameters of heavy charmonia. Huge data samples in 2 – 3 GeV will make it possible to study excited states of  $\rho$ ,  $\omega$  and  $\phi$ , or exotic  $Y(2175)$ ; measure electromagnetic form factor of mesons and baryons; and measure fragmentation functions of hadrons.

## 1 Introduction

Super  $\tau$ -charm factories (STCF) have been proposed in China [1] and Russia [2], presumably to work in 2 – 7 GeV, which is a bridge between the perturbative and non perturbative energy region. It is therefore an important area that is of particular interest for testing QCD predictions. The STCF will be one of the crucial precision frontier for exploring the nature of non-perturbative strong interactions. The experimental data will provide essential information to study QCD dynamics of confinement through the study of hadron spectroscopy. Specifically, high-statistics data will significantly improve the following measurements and studies:

---

\*E-mail: hgs@ustc.edu.cn

- $R$  Measurement
- Measurement of the strong running coupling constant  $\alpha_s$ ;
- Determination of the mass of the charm quark;
- Production cross section of exclusive hadronic channels and the electric and magnetic form factors of light baryons;
- A unique window for charmed baryons;
- Measurement of the inclusive distribution  $x$  and  $\xi$ ;
- Topological event shapes, such as multiplicity, sphericity and thrust.

The Chinese version of STCF is a symmetric electron-positron collider designed to provide  $e^+e^-$  interactions at  $\sqrt{s} = 2.0 \sim 7.0$  GeV. The peaking luminosity is expected to be of  $0.5 \times 10^{35} \text{ cm}^{-2}\text{s}^{-1}$  or higher at  $\sqrt{s} = 4.0$  GeV. The proposed STCF would leave space for higher luminosity upgrades and for the implementation of a longitudinal polarized  $e^-$  beam in a phase-II project.

The STCF detector, a state-of-the-art  $4\pi$ -solid-angle particle detector operating at a high luminosity collider, is a general-purpose detector. It incorporates a tracking system composed of an inner tracker and main drift chamber, a particle identification system, an electromagnetic calorimeter, a super-conducting solenoid, and a muon detector at the outmost. To fully exploit the physics opportunities and cope with the high luminosity, the STCF is designed with following requirements: (nearly)  $4\pi$  solid angle coverage for both charged and neutral particles, and uniform response for these final states; excellent momentum and angular resolution for charged particles, with  $\sigma_p/p = 0.5\%$  at  $p = 1$  GeV/c; high resolution of energy and position reconstruction for photons, with  $\sigma_E/E \approx 2.5\%$  and  $\sigma_{\text{pos}} \approx 5$  mm at  $E = 1$  GeV; superior particle identification ability ( $e/\mu/\pi/K/p/\gamma$  and other neutral particles) and high detection efficiency for low momentum/energy particles; precision luminosity measurement; tolerance to high rate/background environment.

## 2 $R$ measurement

According to quark-parton model, hadrons produced via  $e^+e^-$  collision are characterized by the annihilation of  $e^+e^-$  into a virtual  $\gamma^*$  or  $Z^0$  boson. In the lowest order, the cross section for the (QED) processes  $e^+e^- \rightarrow \gamma^* \rightarrow q\bar{q}$  is related to that for  $e^+e^- \rightarrow \gamma^* \rightarrow \mu^+\mu^-$ ,

$$\sigma(e^+e^- \rightarrow q\bar{q}) = 3 \sum_f Q_f^2 \sigma(e^+e^- \rightarrow \mu^+\mu^-) \quad (1)$$

where  $Q_f$  is the fractional charge of the quark, and three in front records the three colors for each flavor. Summing over all the quark flavors, one defines the ratio of the rate of hadron production to that for muon pairs as

$$R \equiv \frac{\sigma(e^+e^- \rightarrow \gamma^* \rightarrow \text{hadrons})}{\sigma(e^+e^- \rightarrow \gamma^* \rightarrow \mu^+\mu^-)} = 3 \sum_f Q_f^2. \quad (2)$$

The cross section of the pure QED process  $e^+e^- \rightarrow \gamma^* \rightarrow \mu^+\mu^-$  can be precisely calculated, which is the Born cross section  $\sigma(e^+e^- \rightarrow \gamma^* \rightarrow \mu^+\mu^-) = 4\pi\alpha^2/3s$ . Thus, a measurement of total  $e^+e^-$  annihilation cross section into hadron counts directly the number of quarks, their flavor and colors. The  $R$  value is expected to be constant so long as the center-of-mass energy of the annihilated  $e^+e^-$  does not overlap with resonances or thresholds for the production of new quark flavors.

## 2.1 Motivation of the precision measurement of the $R$ values

### 2.1.1 $\alpha(M_Z^2)$ and the Standard Model fits

A remarkable progress has been made in precision test of the Standard Model (SM) during the past thirty years. For the analysis of electroweak data in the SM[3, 4] one starts from the input parameters. Some of them, like  $\alpha(M_Z^2)$ ,  $G_F$ , and  $M_Z$  are very well known, and some others,  $m_{light}$  and  $\alpha_s(M_Z^2)$  are only approximately determined while  $m_t$  and  $m_H$  are still poorly known. Constrain on  $m_t$  and  $m_H$  can be derived by comparing the measured observables with theoretical predictions that has been calculated to full one-loop accuracy and partial two-loop precision, a sufficient precision to match the experimental capabilities.

Out of the three accurately determined quantities  $\alpha(M_Z^2)$ ,  $G_F$ , and  $M_Z$ , the largest uncertainty comes from the running of QED coupling constant  $\alpha(s)$  from  $s = 0$ , where it is known to 0.68 ppb, up to the  $Z$  pole, which is the scale relevant for the electroweak precision test. When relating measurements performed at different energy scales, and if the relation involves  $\alpha(s)$ , one has to know the running of  $\alpha(s)$  in different energy scale. The uncertainty in  $\alpha(M_Z^2)$  arises from the contribution of light quarks to the photon vacuum polarization  $\Delta\alpha(s) = -\Pi_{\gamma\gamma}(s)$  at the  $Z$  mass scale. They are independent of any particular initial or final states and can be absorbed in  $\alpha(s)$

$$\alpha(s) \equiv \frac{\alpha}{1 + \Pi_{\gamma\gamma}(s)} \quad (3)$$

where  $\alpha = 1/137.035999679(94)$ , which is the fine-structure constant, at the precision of 0.68 ppb, and

$$\Delta\alpha(s) \equiv \frac{\alpha(s) - \alpha}{\alpha(s)} = -\Pi_{\gamma\gamma}(s) \quad (4)$$

$\Delta\alpha$  receives the contribution of the leptonic loops and the quark loops to the running

$$\Delta\alpha = \Delta\alpha_l + \Delta\alpha_{had} \quad (5)$$

where the leptonic part  $\Delta\alpha_l$  can be calculated analytically and is well known. The hadronic part  $\Delta\alpha_{had}$  cannot be entirely calculated from QCD because of ambiguities in defining the light quark masses  $m_u$  and  $m_d$  as well as the inherent non-perturbative nature of the problem at small energy scale. An ingenious way[5] is to relate  $\Delta\alpha_{had}$  from quark loop diagram to  $R_{had}$ , as defined by Eqn.2

$$\text{Im}\Pi_{\gamma\gamma}(s) = -\frac{\alpha}{3}R_{had} \quad (6)$$

$$\text{Re}\Pi_{\gamma\gamma}(s) = \frac{\alpha s}{3\pi}P \int_{4m_\pi^2}^{\infty} ds' \frac{R_{had}(s')}{s'(s'-s)}, \quad (7)$$

where  $P$  is the principal value of the integral.

Fig.1 shows the relative contributions to  $\Delta\alpha_{had}^{(5)}(M_Z^2)$  in magnitude and uncertainty [6]. The uncertainty of  $R$  values in the energy region of 2 – 5 GeV is still the second largest contribution to the uncertainty of  $\Delta\alpha_{had}^{(5)}$ . As great effort has been made for improving the  $R$  measurement in the energy region of 1 – 2 GeV, the measurement of  $R$  in 2 – 5 GeV is becoming more and more important again.

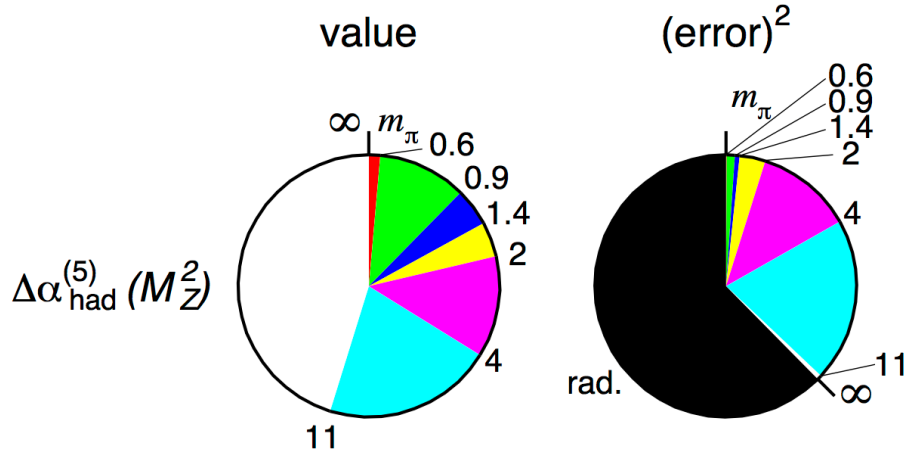


Figure 1: Relative contributions to  $\Delta\alpha_{had}^{(5)}(M_Z^2)$  in magnitude (left) and uncertainty (right) [6].

### 2.1.2 g-2 of the lepton

According to the Dirac theory, a lepton is point-like particle and possesses a magnetic moment

$$\mu = g\mu_B s, \quad (8)$$

where  $\mu_B = e\hbar/2m_e c$  is Bohr magneton and  $s$  the lepton spin.  $g = 2$  for particles of  $s = 1/2$  is predicted by the Dirac theory.

Anomalous magnetic moment of leptons  $a_{lepton} \equiv (g - 2)/2$  receives radiative contributions that can in principle be sensitive to new degree of freedom and interactions. The weak interaction and the vacuum polarization effects are too small to observe for electron because of  $m_l^2$ -dependence. The measurement of  $a_\tau$  is very difficult due to its short lifetime. However, benefited from its larger mass and relatively long lifetime the anomalous magnetic moment of muon  $a_\mu$  has been measured with very high precision at the CERN Muon Storage Ring[7, 8, 9], and recently by E821 experiment done at Brookhaven National Laboratory to a precision of 0.5 ppm[10], which is one of the best measured quantities in physics. Theoretically,  $a_\mu$  is sensitive to large energy scales and very high order radiative corrections [11, 12]. It therefore provides an extremely clean test of electroweak theory and may give us hints on possible deviations from the SM [13, 14, 15].

According to different source of contribution,  $a_\mu$  can be decomposed as

$$a_\mu^{the} = a_\mu^{QED} + a_\mu^{had} + a_\mu^{weak} + a_\mu^{new}. \quad (9)$$

The QED contribution, the largest term among all, has been calculated to  $\mathcal{O}(\alpha^5)$ , including the contribution from  $\tau$  vacuum polarization.  $a_\mu^{weak}$  includes the SM effects due to virtual W, Z and Higgs particle exchanges.  $a_\mu^{had}$  denotes the virtual hadronic (quark) contribution determined by QCD, part of which corresponds to the effects representing the contribution of running  $\alpha(s)$  from low energy to high energy scale. It cannot be calculated from first principle but relates to the experimentally determined  $R_{had}(s)$  through the expression

$$a_\mu^{had} = \left(\frac{\alpha m_\mu}{3\pi}\right)^2 \int_{4m_\pi^2}^{\infty} ds \frac{R_{had}(s)K(s)}{s^2} \quad (10)$$

where  $K(s)$  is a kernel varying from 0.63 at  $s = 4m_\pi^2$  to 1.0 at  $s = \infty$ .  $a_\mu^{new}$  stands for the possible contributions beyond the SM, which is assumed to be zero so far.

The fractional contributions to the total mean value and uncertainty of  $a_\mu^{had}$  from various energy intervals is shown in Figure 2 [6].

The hadronic vacuum polarization is the most uncertain one of all the SM contributions to  $a_\mu$ . For several scenarios, it has been claimed 30 years ago that "the physics achievement of the effort to re-measure the cross section of  $e^+e^-$  hadrons that brings down the uncertainty of  $a_\mu$  to  $60 \times 10^{-11}$  is equivalent to that of LEP2 or even

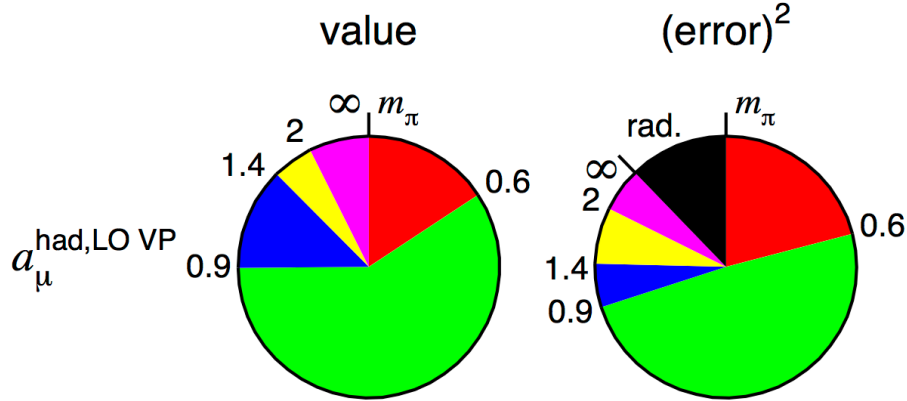


Figure 2: Relative contributions to  $a_\mu^{\text{had}}$  in magnitude (left) and uncertainty (right) [6].

LHC” [13, 16]. Now after 30 years effort from both theory and experiments, the uncertainty on  $a_\mu$  has been evaluated to be  $a_\mu(\text{SM}) = 116591810(43) \times 10^{-11}$  [17], bringing down the uncertainty to 0.37 ppm. The new experiment P989 at Fermilab measured  $a_\mu$  to be  $116592040(54) \times 10^{-11}$  (0.46 ppm) [18], and it becomes  $116592061(41) \times 10^{-11}$  (0.35 ppm) [18] if combined with previous results. So the theoretical prediction lags behind, once again calls for further reducing the uncertainties of the  $R$  values in the energy region below 5 GeV.

Near the threshold, as seen from Eqn.7 and Eqn.10, the integration is proportional to  $R_{had}/s^2$ , whereas the  $\Delta\alpha(M_Z)$  integration is proportional to  $R_{had}/s$ . This implies that  $a_\mu^{\text{had}}$  is more sensitive to the lower energy than to the higher one. Measurement in the energy region of 0.5 – 1.5 GeV from VEPP-2M in Novosibirsk and  $\phi$  factory at DA $\phi$ NE greatly contributed to the interpretation of  $g - 2$  measurement at Brookhaven[10] and Fermi Lab [18]. However, their contribution to the precision determination of  $\alpha(M_Z)$  is limited. The  $R$  value from BESII at BEPC in the energy region of 2 – 5 GeV made the major contribution to evaluate  $\alpha(M_Z)$ , and also partly contributed to the interpretation of  $g-2$ . New measurement of  $R$  value is highly anticipated at a future super  $\tau - c$  factory.

## 2.2 Current status and potential to measure $R$

Experimentally the  $R$  value is determined as following,

$$R = \frac{\sigma_{had}^0}{\sigma_{\mu\mu}^0} = \frac{N_{had}^{obs} - N_{bg} - \sum_l N_{ll} - N_{\gamma\gamma}}{\sigma_{\mu\mu}^0 \cdot L \cdot \bar{\epsilon}_{had} \cdot \epsilon_{trg} \cdot (1 + \delta)}, \quad (11)$$

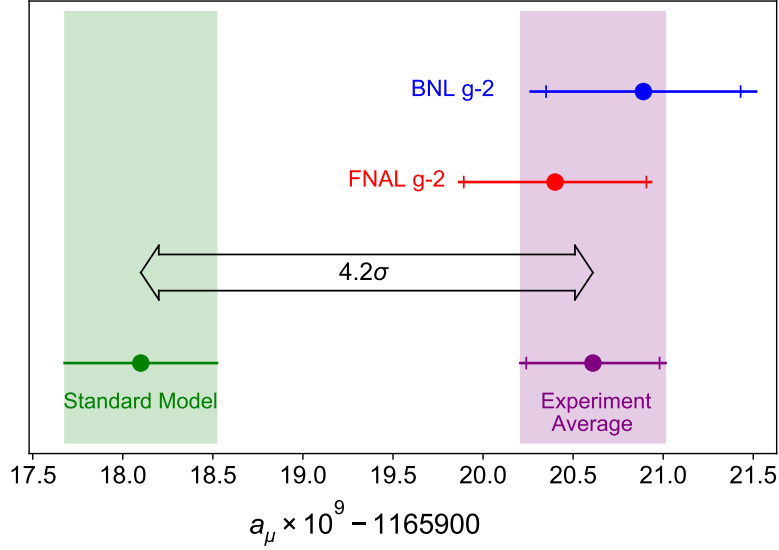


Figure 3: Anomalous magnetic moment of leptons predicted by the SM and measured by the experiment [18].

where  $1 + \delta$  is a factor taking the radiative correction into account for the initial states.  $N_{had}^{obs}$  is the number of hadronic events collected during a colliding-beam run at a certain energy with integrated luminosity  $L$  and survived after applying the hadronic events selection criteria. To obtain  $\sigma_{had}^0$ ,  $N_{had}^{obs}$  must be corrected for background from different sources. The beam associated background  $N_{bg}$  will be estimated from separated-beam data recorded at each energy to be measured.  $N_{ll}(l = e, \mu, \tau, \gamma)$ , the background contributed from lepton pair production and two-photon process can be estimated by Monte Carlo simulation.

On the other hand, the higher order QCD corrections to  $R$  has also been calculated in complete 3rd order perturbation theory[19], and the results can be expressed as

$$R = 3 \sum_f Q_f^2 \left[ 1 + \left( \frac{\alpha_s(s)}{\pi} \right) + 1.411 \left( \frac{\alpha_s(s)}{\pi} \right)^2 - 12.8 \left( \frac{\alpha_s(s)}{\pi} \right)^3 + \dots \right] \quad (12)$$

where  $\alpha_s(s)$  is the strong coupling constant. Precise measurement of  $R$  can be employed to determine  $\alpha_s$  according to Eqn. 12, which exhibits a QCD correction known to  $\mathcal{O}(\alpha_s^3)$ . In addition, at low c.m. energy, non-perturbative corrections (e.g. resonances, etc.) could be important.  $R$  has been measured by many laboratories in the energy region covering from hadron production threshold to the  $Z^0$  pole[20]. The results are shown in Fig.4.

The uncertainties of  $R$  in different energy region are summarized in Table 1. The uncertainty of  $R$  at the center-of-mass energy between 1 and 2 GeV is about 10-15%,

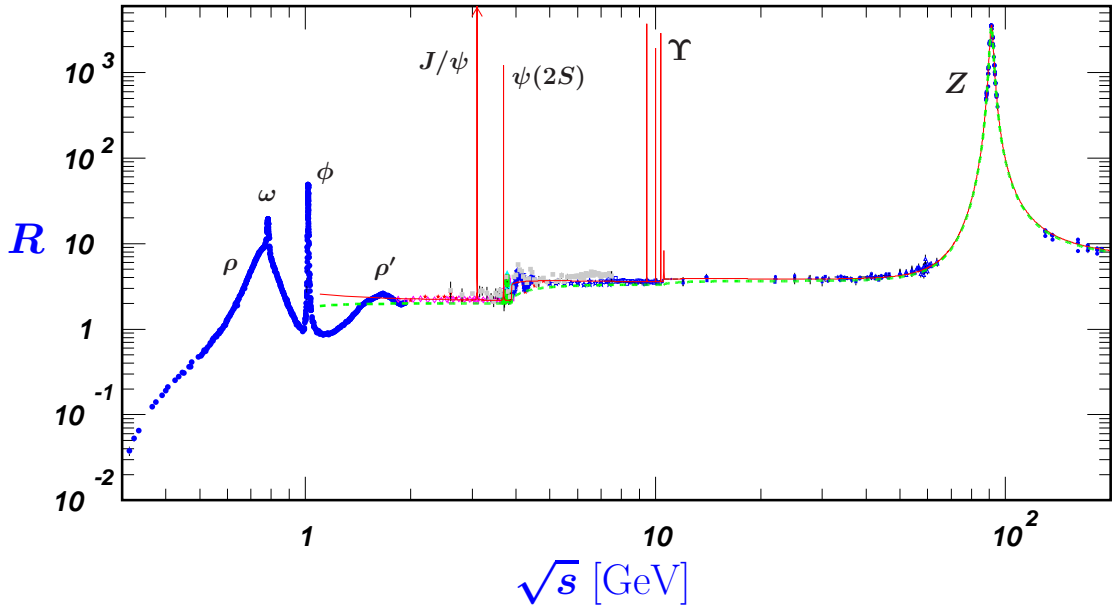


Figure 4:  $R$  in  $e^+e^-$  collision[20].

for the energy between 2 and 5 GeV, the uncertainty of  $R$  has been reduced from over 15% [21, 22, 23, 24] to about 6% after a  $R$  scan was performed with BESII at BEPC [25]. Between the charm and bottom thresholds, i.e., about 5 – 10.4 GeV,  $R$  were measured by Mark I, DASP, PLUTO, Crystal Ball, LENA, CUSB, DESY-Heidelberg, DM-1 [26], CLEO [27] collaborations. Their systematic normalization uncertainties were about 5 – 10%. Above bottom threshold, the measurements were from PEP, PETRA and LEP with uncertainties of 2 – 7%.

Table 1: Typical uncertainties of  $R$  in different energy region [20].

Ecm (GeV)	< 1	1 – 2	2 – 5	5 – 7	10 – $m_Z$
$\Delta R/R$ (%)	0.9	15	3 ~ 6	6	2 ~ 7

Fig.5 quoted from Ref.[20] shows the  $R$  values for center-of-mass energies up to 5 GeV, including resonances. The experimental  $R$  values are in general consistent with theoretical predictions, which are impressive confirmation of the hypothesis of three color degrees of freedom for quarks.

In recent a few years, KEDR measured  $R$  values between 1.84 and 3.72 GeV with uncertainties around 3% ~ 4% [28, 29, 30]. BESIII just published its first  $R$  measurements between 2.23 and 3.67 GeV with precision better than 3% [31]. These results are shown in Fig.6.

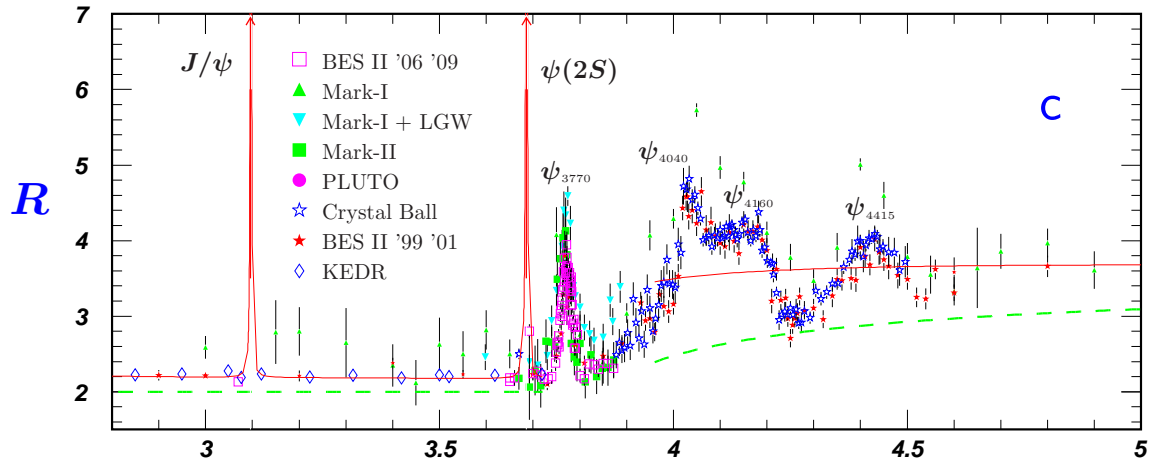


Figure 5:  $R$  in light-flavor and charm energy region[20].

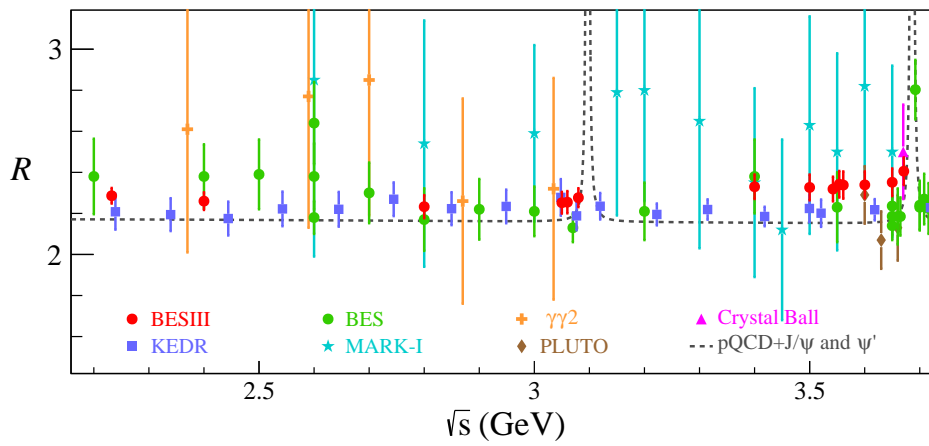


Figure 6:  $R$  in continuum region[31].

## 2.3 Heavy charmonia

DASP group[32] inferred the existence of narrow resonance at 4.04 GeV and 4.16 GeV. In addition to the resonance at 3.77 GeV, Mark I data[33] shown a broad enhancement at 4.04, 4.2 and 4.4 GeV. The resonance at 4.4 GeV was also observed by PLUTO[34], but the height and width of the resonance were reported differently. The broad resonances at 4.04, 4.16 and 4.45 have been clearly observed by BES Collaboration from the  $R$  scan data, and their resonance parameters have been measured with improved precision[35] by fitting to the inclusive  $R$  spectrum as shown in Fig.7. CLEO-c has done a  $R$  scan with only 13 energy points, which has shown the resonances of  $\psi(4040)$ ,  $\psi(4160)$ [36]. Using ISR, Belle has reported a measurement of exclusive channels and added them up to compare with  $R$ [37].

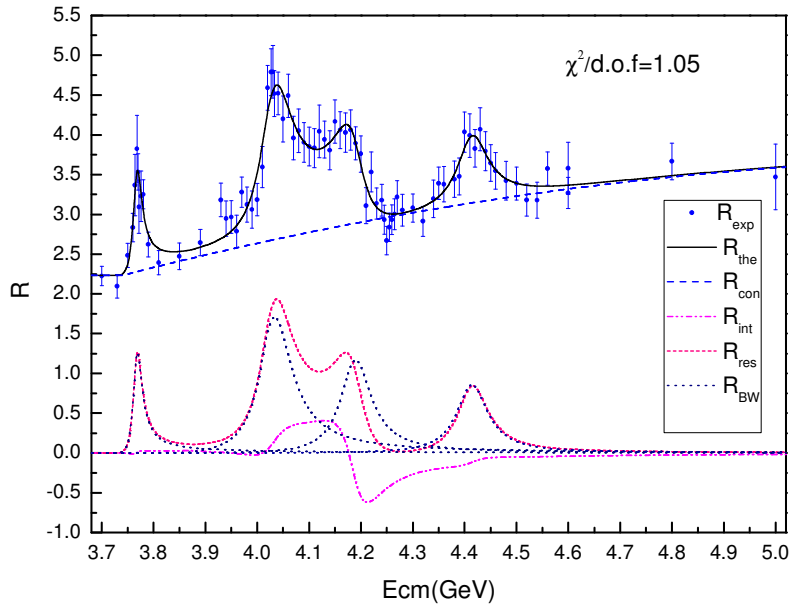


Figure 7: Fit to the BESII  $R$  spectrum with all two body decays of  $\psi(3770)$ ,  $\psi(4040)$ ,  $\psi(4160)$  and  $\psi(4415)$ . Interference among the resonances and the phase have significant effect on the fitting.

Though the broad resonances at 4040, 4160 and 4415 MeV are assigned to be the high mass charmonia, we don't have much experimental information for understanding them. Their widths are poorly measured, and their decay channels are not well studied. Therefore, a high precision  $R$  scan in the 3.9 – 4.6 GeV region would be very valuable in disentangling the physics of that region.

## 2.4 R from pQCD and measurement of $\alpha_s$

A precision measurement of  $R$  values is a direct test of QCD. According to Eqn.12, the strong coupling constant  $\alpha_s(s)$  can be determined with  $R$  values[19, 38, 39].

## 2.5 Determination of the mass of the charm quark

With the help of QCD sum rules, the charm quark mass can be determined using the  $R$  values. There are different ways to define the quark mass. The one in  $\overline{\text{MS}}$  scheme is often written as  $m_c(m_c)$ , or  $m_c(\mu)$  at a chosen energy scale  $\mu$  which should be high enough to ensure convergence of the perturbative series. Another form is the pole mass, denoted as  $M_c$ . Soon after BESII  $R$  values were released, a number of evaluations of the charm quark mass were reported[40, 41]. The new precision measurement of  $R$  values at BESIII will once again draw the attention of theorists in the area, and we may want to determine the charm quark mass by ourselves as well.

## 2.6 Predictions from MLLA/LPHD

Perturbative QCD can give quantitative analytical predictions based on the modified leading logarithmic approximation (MLLA)[42] under the assumption of local parton hadron duality (LPHD)[43]. At high energies, there are sufficient experimental results, but it is not the case for low energies. BESII provided first measurements of inclusive momenta, multiplicity, the second binomial moments in the energy region of 2 – 5 GeV[44]. To better test the QCD predictions, more accurate measurements with uncertainty of a few percent are expected at BESIII.

## 2.7 Hadronic form factors

The electromagnetic form factors (EM FF's) is a fundamental observable of QCD and describes the internal structure of the hadron. It also provides a way to understand its dynamics. The proton is one of the basic building blocks of matter and its EM FF's are necessary for the interpretation of many theory problems and experimental measurements involving strong interactions. The form factors are calculated in the non-perturbative region in the field theory, where the free parameters in the semi-phenomenological expression obtained from QCD have to be measured experimentally. The proton form factor can be measured in the space-like region (SL) by studying elastic electron-proton scattering, and the time-like region (TL) by proton-antiproton production in electron-positron annihilation.

The major part of the existing data bank concern SL FF's, while TL FF measurements are scarce and with large uncertainties. BESII measured the proton form factor at 10 energy points in 2 – 3.07 GeV, but with large statistical uncertainties[45]. BESIII

continued the effort and extracted the form factors of proton and neutron with unprecedented precision. For more rigorous constraints on QCD phenomenological models, further improvements are highly desired at future STCF.

For a coherent picture of the low mass spin 1/2 baryon octet, the time-like form factors of hyperons are also needed:  $\Lambda$ ,  $\Sigma$  and  $\Xi$ . BESIII already made contributions, but apparently STCF is more superior with regard to statistics. Due to the finite lifetime of hyperons, it is not possible to construct hyperon targets, and observables like space-like form factors, Transverse Momentum Distributions (TMD's) or Generalized Parton Distributions (GPD's) are not accessible. Time-like form factor is therefore the most powerful way to study hyperon structure. The key question in hyperon structure physics is “*What happens, if a light quark in the nucleon is replaced by a heavier one?*”. If SU(3) symmetry was exact, the properties of hyperons could be derived from those of the nucleons. By comparing the structure of nucleons and hyperons, we can learn to what extent SU(3) symmetry is broken and the impact of a heavier quark in a system of light quarks. Form factors in the time-like region are complex and the electric and the magnetic form factor have a relative phase. This has a polarisation effect on the final state even if the initial  $e^+e^-$  state are unpolarised. The weak, parity violating decay of hyperons, that causes the decay particles to be emitted in the direction of the spin of the hyperon, makes the polarisation of the hyperon experimentally accessible [46]. This gives a unique feature of the hyperons: the time-like form factors can be fully determined.

### 3 The strangeonium

The strangeonium ( $s\bar{s}$ ) states [47] have not been known well like Charmonium ( $c\bar{c}$ ) and bottomonium ( $b\bar{b}$ ). So far the spectrum of strangeonium has not been established well, both in theory predictions and in experimental observations. Below 2.2 GeV, there should be 22  $s\bar{s}$  resonances expected, but unfortunately only about half of them are identified. One reason might be, due to the smaller mass of the  $s$  quark, the strangeonium states are over crowded in the low energy region, and mixed with hybrids, glueballs and other exotics.

The  $\phi(2170)$ , most probably a strangeonium state but previously referred to as the Y(2175) [48], has been observed experimentally by *BABAR* [49, 50], Belle [51], BES [52] and BESIII [53, 54]. However the information is diverse, and even the measured mass and width of  $\phi(2170)$  are controversial. There have also been different models for  $\phi(2170)$ , such as traditional  $3\ ^3S_1$  [55] or  $2\ ^3D_1\ s\bar{s}$  [56] state,  $1^{--}\ s\bar{s}g$  hybrid [57, 58], tetraquark state [59, 60, 61, 62, 63],  $\Lambda\bar{\Lambda}(^3S_1)$  bound state [64, 65, 66, 67],  $S$ -wave threshold effect [68], or  $\phi K\bar{K}$  resonance state [69].

To improve the knowledge, BESIII measured a number of processes, including  $e^+e^- \rightarrow K^+K^-$  [70],  $e^+e^- \rightarrow K_S^0K_L^0$  [71],  $e^+e^- \rightarrow K^+K^-\pi^0\pi^0$  [72],  $e^+e^- \rightarrow K^+K^-K^+K^-/$

$\phi K^+ K^-$  [73],  $e^+e^- \rightarrow \phi\eta$  [74],  $e^+e^- \rightarrow \phi\eta'$  [75],  $e^+e^- \rightarrow \omega\eta/\pi^0$  [76], using data collected in the center-of-mass energy region of 2.0–3.08 GeV,. These experimental results provide additional information in understanding the  $\phi(2170)$ . The current situation of the  $\phi(2170)$  parameters is displayed in Fig. 8, indicating the  $\phi(2170)$  remains intriguing and therefore more efforts are needed. Hopefully a STCF will eventually settle it down and identify more strangeonium states in the future.

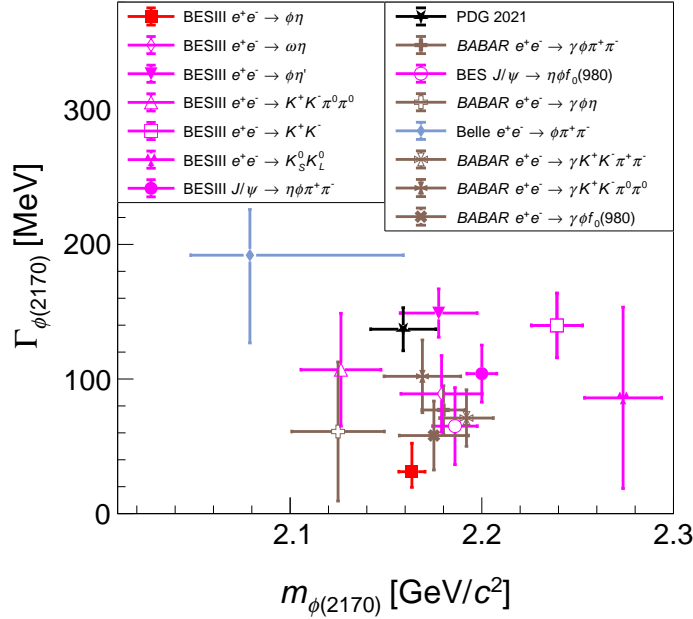


Figure 8: A compilation of measured mass and width of the  $\phi(2170)$ .

## 4 Fragmentation function

Fragmentation function (FF)  $D_q^h(z)$  is the probability that hadron  $h$  is found in the debris of a quark (or antiquark) carrying a fraction  $z$  of its energy. The corresponding differential cross section can be written as

$$\frac{d\sigma(e^+e^- \rightarrow h + X)}{dz} = \sum_q \sigma(e^+e^- \rightarrow q\bar{q})(D_q^h(z) + D_{\bar{q}}^h(z)) \quad (13)$$

at leading level [77]. The fragmentation function  $D_q^h(z)$  is a nonperturbative object due to hadronization, and can not be deduced from first principles, but could be extracted from experimental data on inclusive hadron production.

At BESIII fragmentation functions have been measured from inclusive  $\pi^0$  and  $K_S^0$  productions in the c.m. energy range between 2.2324 to 3.6710 GeV with statistical uncertainties comparable to systematic ones. These measurements fill the area below 10 GeV, where there were almost no experimental data. The results offer unique opportunity to extract the unpolarized fragmentation functions in the relatively low energy region and to study the QCD dynamics in this particular region.

## 5 Nucleon form factors

The ratio of proton electromagnetic form factors ( $R_{\text{em}}$ ) in the time-like region (TL) was in poor accuracy ranging between 12% and 28%, increasing with increasing momentum transferred by the virtual photon,  $q$ . Before BESIII, there were only two experiments which measured  $R_{\text{em}}$ : BaBar [78, 79] and PS170 [80]. BaBar measured  $R_{\text{em}}$  in six different  $q$ -bins via the process  $e^+e^- \rightarrow p\bar{p}\gamma$ . The  $q$ -region covered by BaBar was between 1.877 and 3.0 GeV. PS170 measured the process  $p\bar{p} \rightarrow e^+e^-$  in five fine  $q$ -bins between 1.931 and 2.049 GeV. While the spectrum of the PS170 experiment seems to be compatible with the assumption  $|G_E|/|G_M| = 1$ , the BaBar spectrum shows a relatively large deviation from 1, measuring values of  $|G_E|/|G_M|$  greater than unity. In the case of the neutrons, there was no independent measurement of the electromagnetic form factors or their ratio so far. Only FENICE-experiment [81] in Frascati extracted the neutron form factor  $G_M^n$  from the measurement of the cross section in the reaction  $e^+e^- \rightarrow n\bar{n}$  and assuming  $G_E^n = 0$ .

### 5.1 Nucleon electromagnetic form factors in the TL region

Electromagnetic form factors (FFs) account for the non point-like structure of hadrons. The vertex operator  $\Gamma^\mu(q)$  describing the hadronic current in the Feynman diagrams of Fig. 9 can be written in terms of the so called Dirac and Pauli FFs,  $F_1$  and  $F_2$ :

$$\Gamma^\mu(q^2) = \gamma^\mu F_1(q^2) + \frac{i\sigma^{\mu\nu}q_\nu}{2m_N} F_2(q^2), \quad (14)$$

with  $m_N$  the mass of the nucleon  $N$  or spin-1/2 baryon. The FFs are analytic functions of the momentum transferred  $q^2$ . They are real in the space-like (SL) region ( $q^2 < 0$ ) and can be complex in the time-like (TL) region ( $q^2 > 0$ ) for  $q^2 > 4m_\pi^2$ . The use of the so-called Sachs FFs has become conventional:

$$G_E(q^2) = F_1(q^2) + \frac{q^2}{4m^2} F_2(q^2), \quad G_M(q^2) = F_1(q^2) + F_2(q^2), \quad (15)$$

with  $G_E(0) = G_M(0)/\mu_N = 1$  and  $\mu_N$  the nucleon magnetic moment. Form factors for  $q^2 < 0$  are determined by elastic scattering of electrons from hadrons available as

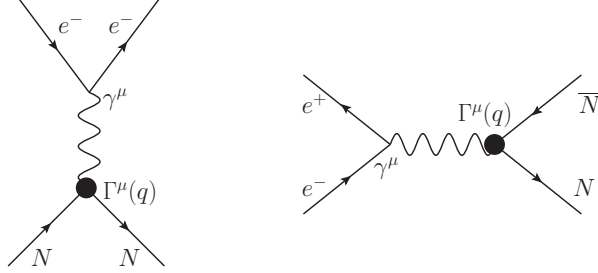


Figure 9: Lowest-order Feynman diagrams for  $e^- N \rightarrow e^- N$  (left) and for  $e^- e^+ \rightarrow N \bar{N}$  (right).

targets. Form factors for  $q^2 > 0$  are measured in annihilation processes  $e^+ e^- \leftrightarrow N \bar{N}$ . The differential cross section of the annihilation process  $e^+ e^- \rightarrow N \bar{N}$  in c.m. [82] reads

$$\frac{d\sigma(q^2, \theta_N^{CM})}{d\Omega} = \frac{\alpha^2 \beta C}{4q^2} \left[ (1 + \cos^2 \theta_N^{CM}) |G_M(q^2)|^2 + \frac{1}{\tau} \sin^2 \theta_N^{CM} |G_E(q^2)|^2 \right], \quad (16)$$

where  $q^2 = M_{pp}^2$  is the momentum transferred by the virtual photon,  $\theta_N^{CM}$  is the polar angle of the nucleon,  $\tau = 4m_N^2/q^2$ ,  $m_N$  is the mass of the nucleon,  $\beta = \sqrt{1 - 1/\tau}$ ,  $C = y/(1 - \exp(-y))$  and  $y = \pi\alpha/\beta$ . The Coulomb factor  $C$  accounts for the electromagnetic  $N\bar{N}$  interactions [83]. The analysis of the angular differential cross section allows the independent extraction of the electromagnetic form factors  $G_E$  and  $G_M$ . Angular integration of the previous equation gives the total cross section:

$$\sigma(q^2) = \frac{4\pi\alpha^2\beta C}{3q^2} \left[ |G_M(q^2)|^2 + \frac{1}{2\tau} |G_E(q^2)|^2 \right]. \quad (17)$$

## 5.2 Extraction of $R_{em} = |G_E|/|G_M|$ and $G_{E,M}$

In order to extract the ratio of the electromagnetic form factors, the proton angular distributions of the selected events are weighted with the selection efficiencies with rad. corr. and fitted with the following formula:

$$f(\cos\theta_p^{CM}) = Norm \cdot [\tau(1 + \cos^2\theta_p^{CM}) + R_{em}(1 - \cos^2\theta_p^{CM})], \quad (18)$$

with two free parameters, a global normalization factor,  $Norm$ , and the ratio of the electromagnetic form factors  $R_{em}$ . This formula is equivalent to Eq. 16 after factorizing out  $|G_M|$ . The electromagnetic form factors can be extracted as:

$$|G_M|^2 = \frac{Norm \cdot 2q^2\tau}{L \cdot bw \cdot \pi\alpha^2\beta}, \quad (19)$$

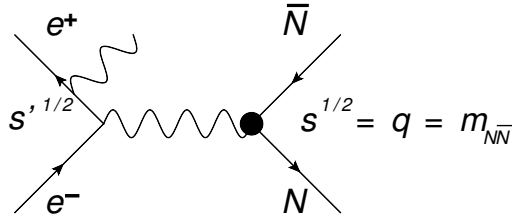


Figure 10: One of the lowest-order Feynman diagrams for initial-state radiation emission in  $e^+e^- \rightarrow p\bar{p}$ .

$$|G_E|^2 = |R_{\text{em}}|^2 \cdot |G_M|^2, \quad (20)$$

where  $L$  is luminosity and  $\text{bw}$  is bin width. Due to the factor  $1/\tau$  in front of  $|G_E|^2$  in Eq. 16, this form factor is strongly suppressed at high  $q^2$ .

### 5.3 ISR vs energy-scan

Taking advantage of the ISR-technique (Fig. 10), the whole range below a fixed nominal energy would be accessible. As indicated by Eq. 21,  $L_{\text{ISR}}(\sqrt{s}, E_\gamma)$ , and  $L_0(\sqrt{s})$  are the ISR-Luminosity at  $q = \sqrt{s}$  and the luminosity at at the same  $q$  for the direct annihilation, respectively. The use of the ISR-technique to measure electromagnetic nucleon form factors would allow to measure the electromagnetic form factors in bins of non-negligible finite size of  $q^2$ , but not in differential  $q^2$ -bins.

$$L_{\text{ISR}}(\sqrt{s}, E_\gamma) = \beta \frac{dE_\gamma}{E_\gamma} \left[ 1 - \frac{dE_\gamma}{E_\gamma} + \frac{1}{2} \left( \frac{dE_\gamma}{E_\gamma} \right)^2 \right] \cdot d\sqrt{s'} \cdot L_0(\sqrt{s}), \quad (21)$$

with  $E_\gamma = \sqrt{s'}/2 \cdot (1 - m_{N\bar{N}}^2)$  the energy of the real photon and  $m_{N\bar{N}}$  the invariant-mass of the  $N\bar{N}$ -system.

## 5.4 Nucleon form factors at BESIII

### 5.4.1 Proton

BESIII obtained the most accurate proton  $|G_E/G_M|$  ratio measurements at 16 c.m. energies between 2.0 and 3.08 GeV [84, 85] that favor BaBar over PS170 and helped clarifying the puzzle. BESIII also performed the measurements using the ISR technique [86, 87], with results that are consistent with BaBar's. The BESIII measurements are shown in Fig. 11 (a) for  $p\bar{p}$  production cross section in 2.0 – 3.08 GeV, (b) the effective proton time-like form factor, (c) the form factor ratio  $R = |G_E/G_M|$ , and (d) the

effective form factor residual, together with results from other experiments. The electric form factor was extracted for the first time. The unprecedented 3.5% uncertainty that was achieved at 2.125 GeV by BESIII is close to that of the best measurements in the space-like region, which have been at per cent level since long time ago. The CMD-3 experiment measured the production cross section of proton pair and observed an abrupt rise at the nucleon-antinucleon threshold [88], as expected for point-like charged particles according to Eqn. 16. BESIII did not extend down to the threshold energy, but the results around 2 GeV agree with CMD-3. This information improves our understanding of the proton inner structure from a different dimension and helps to test theoretical models that depend on non-perturbative QCD, e.g. charge distribution within the proton can be deduced [89, 90]. The near threshold behavior of the electromagnetic form factor of a hadron is mostly determined by the interaction of the hadron-antihadron in the final state, and therefore the measurements of the form factor properties can also serve as a fruitful source of information about hadron-antihadron interaction [91].

Interestingly there are oscillations in the effective proton form factor, first seen by BaBar and later confirmed by BESIII [86]. These oscillations were subsequently studied with more precise data by BESIII [85]. Ref. [92] speculated that possible origins of this curious behavior are rescattering processes at relative distances of 0.7 - 1.5 fm between the centers of the forming hadrons, leading to a large fraction of inelastic processes in  $p - \bar{p}$  interactions, and a large imaginary component to the rescattering processes.

### 5.4.2 Neutron

The most recent measurement of the TL neutron FFs was performed at the BESIII experiment. A data set with a total integrated luminosity of 647.9 pb<sup>-1</sup> at 18 energies between  $\sqrt{s} = 2.0$  and 3.08 GeV was used and over 2000  $n\bar{n}$  events were selected to determine  $\sigma_B^{n\bar{n}}$  and  $|G^n|$ . Because the final state neutron and anti-neutron are both neutral, with no tracks recorded in the drift chamber, the event selection is a challenge. The information in the calorimeter and the time of flight counters has to be used to identify the signal; as such the selection efficiency is much lower and the number of observed neutron events is significantly less than that for protons. The results were published in 2021 [93] and represent the most precise and extensive measurement up to date. The precision of  $\sigma_B^{n\bar{n}}$  is greatly improved when compared to previous measurements. The accuracy of  $\sigma_B^{n\bar{n}}$  ranges between  $\sim 4\text{--}40\%$  and  $\sim 6\text{--}16\%$  from statistics and systematic effects, respectively. The results from BESIII on  $\sigma_B^{n\bar{n}}$  and  $|G^n|$  are shown in Fig. 12.

Neutron measurements from SND [94, 95] and BESIII [93] overlap and roughly agree at 2 GeV, where a cross-section behavior that is close to the  $e^+e^- \rightarrow p\bar{p}$  case is observed, in particular a flat behavior above threshold up to 2 GeV as seen by CMD-3 [88], but this challenges the expected behavior from Eqn. 16. For energies above 2 GeV, the BESIII measurements of the ratio of the proton to neutron cross sections is more compatible with the QCD-motivated model predictions: as shown in Fig. 13, the cross section for

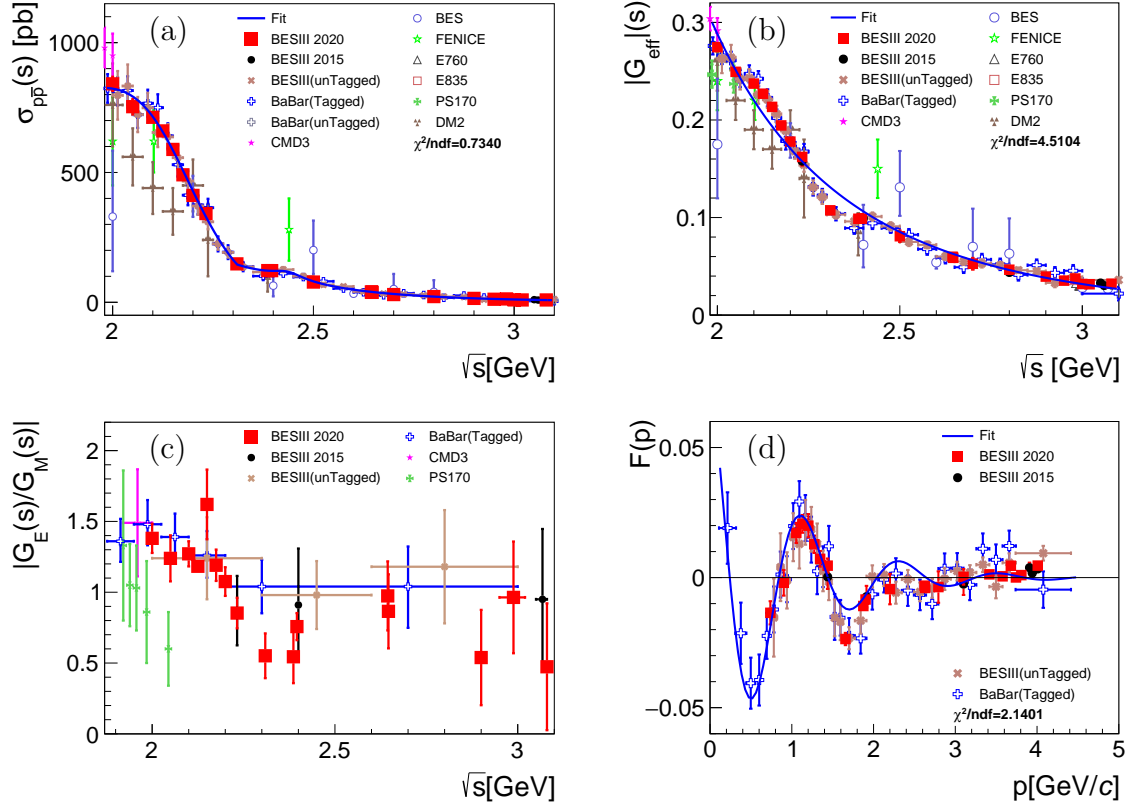


Figure 11: (a) the cross sections for  $e^+e^- \rightarrow p\bar{p}$  cross section. (b) the effective proton time-like form factor. The blue curve is the results of an attempt to fit the measurements with smooth dipole-like function. (c) the ratio  $R = |G_E/G_M|$ . (d) effective form factor residual  $F(p)$  after subtracting the one calculated by QCD theory (the blue curve shown in (b)), as a function of the relative motion  $p$  of the final proton and antiproton.

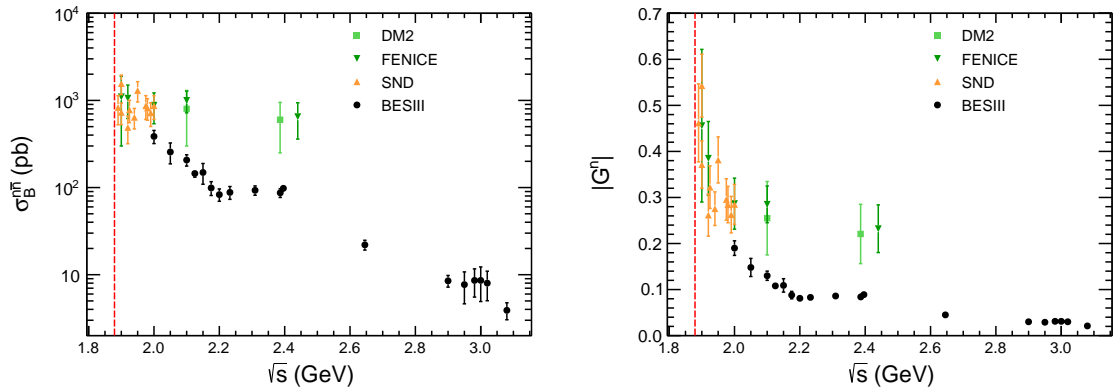


Figure 12: **Left:** Results for the Born cross section  $\sigma_B^{n\bar{n}}$  with respect to the center-of-mass energy  $\sqrt{s}$ . **Right:** Results for the effective form factor  $|G^n|$  with respect to the center-of-mass energy  $\sqrt{s}$ .

$e^+e^- \rightarrow p\bar{p}$  is larger than for  $e^+e^- \rightarrow n\bar{n}$  in general.

## 6 Hyperon threshold effects

The  $\Lambda$  was measured previously by the DM2 [96] and BaBar [97] experiments. BESIII studied the channel  $e^+e^- \rightarrow \Lambda\bar{\Lambda}$  [98] with a  $40.5 \text{ pb}^{-1}$  data sample collected at four different energy scan points. The lowest energy point is 2.2324 GeV, only 1 MeV above the  $\Lambda\bar{\Lambda}$ -threshold. These data made it possible to measure the Born cross section very near threshold. To use the data as efficiently as possible, both events where  $\Lambda$  and  $\bar{\Lambda}$  decayed to the charged mode ( $\text{Br}(\Lambda \rightarrow p\pi^-) = 64\%$ ) and events where the  $\bar{\Lambda}$  decayed to the neutral mode ( $\text{Br}(\bar{\Lambda} \rightarrow \bar{n}\pi^0) = 36\%$ ) were selected. In the first case, the identification relied on finding two mono-energetic charged pions with evidence for a  $\bar{p}$ -annihilation in the material of the beam pipe or the inner wall of the tracking chamber. In the second case, the  $\bar{n}$ -annihilation was identified with a multi-variate analysis of variables provided by the electromagnetic calorimeter. Additionally, a mono-energetic  $\pi^0$  was reconstructed to fully identify this decay channel. For the higher energy points, only the charged decay modes of  $\Lambda$  and  $\bar{\Lambda}$  were reconstructed by identifying all the charged tracks and using the event kinematics. The resulting measurement [98] of the Born cross section are shown in Fig. 14 together with previous measurements [96, 97]. The Born cross section near threshold is found to be  $312 \pm 51(\text{stat.})_{-45}^{+72}(\text{sys.}) \text{ pb}$ . This result confirms BaBar's measurement [97] but with much higher momentum transfer squared accuracy. Since the Coulomb factor is equal to 1 for neutral baryon pairs, the cross section is expected to go to zero at threshold. Therefore the observed threshold enhancement implies the existence of a complicated underlying physics scenario. The unexpected features of

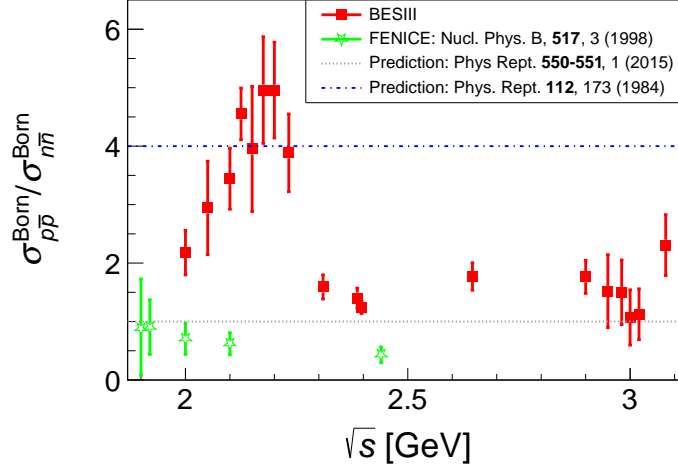


Figure 13: Ratio of Born cross section of  $e^+e^- \rightarrow p\bar{p}$  to that of  $e^+e^- \rightarrow n\bar{n}$ .

baryon pair production near threshold have driven a lot of theoretical studies, including scenarios that invoke bound states or unobserved meson resonances [91, 99, 100]. It was also interpreted as an attractive Coulomb interaction on the constituent quark level [101, 102]. Another possible explanation is the final-state interactions which play an important role near the threshold [103, 104, 105].

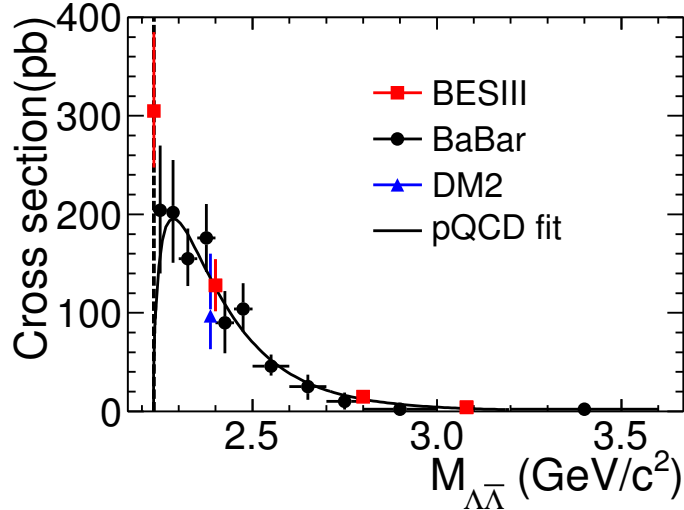


Figure 14: Cross section of  $e^+e^- \rightarrow \Lambda\bar{\Lambda}$ .

The spike and the non zero cross section are a big surprise, since this cross section

was expected to be vanishing, because of the phase space factor, the baryon center of mass (c.m.) velocity  $\beta$ . It is the same for any neutral particle pair production at threshold. On the contrary a jump is expected in the case of charged fermion, lepton or baryon, pairs. In fact the final state long range Coulomb interaction introduces in the cross section a factor proportional to  $\beta^{-1}$ , which cancels the phase space factor  $\beta$ . This argument is exploited in some more detail in the following.

In the case of a lepton pair an additional final state Coulomb factor  $\mathcal{C}$  is predicted [106], the so called Sommerfeld-Schwinger-Sakharov rescattering formula. This factor has a very weak dependence on the fermion pair total spin, hence it is assumed to be the same for form factors (FF)  $G_E$  and  $G_M$ . With a good, non-relativistic, approximation it is:

$$\mathcal{C} = \frac{\pi\alpha}{\beta} \frac{1}{1 - \exp(-\pi\alpha/\beta)}.$$

There are various relativistic small improvements of this formula, like the substitution  $\beta \rightarrow \tilde{\beta} = \beta/(1 - \beta)$ , which has been applied in the following. This  $\mathcal{C}$  factor can also be obtained introducing the Coulomb final state interaction as the wave function at the origin squared in  $p\bar{p}$  scattering. Therefore such a Coulomb factor should affect the S wave.

Essentially the  $\beta^{-1}$  divergency comes from the one photon exchange and the so called resummation factor  $\mathcal{R} = [1 - \exp(-\pi\alpha/\tilde{\beta})]^{-1}$  takes into account the many photons exchange. The resummation factor for pointlike fermions is so that the phase space  $\beta$  and the corresponding fast increase in the cross section are restored after few MeV. Because of the finite colliding beams energy spread the Coulomb steep rise is hardly seen in the case of lepton pairs, like  $\mu^+\mu^-$  or  $\tau^+\tau^-$ .

Hence the clear evidence of a jump in the case of  $e^+e^- \rightarrow p\bar{p}$ , followed by a flat cross section up to about 2100 MeV in the c.m., is very consistent with the absence of an electromagnetic  $\mathcal{R}$  in the case of a charged baryon pair production. In fact in this case also strong interactions, that is gluon exchange, must contribute to  $\mathcal{R}$ . Assuming  $\mathcal{R}_s = [1 - \exp(-\pi\alpha_s/\tilde{\beta})]^{-1}$ , with  $\alpha_s$  about 0.5, the flat  $e^+e^- \rightarrow p\bar{p}$  cross section on a hundred MeV scale is well reproduced. By the way S wave dominance at threshold is required also by analyticity and, as a consequence, there should be one FF, since both imply that  $G_E^p(4M_p^2) = G_M^p(4M_p^2)$ , at least close to the threshold.

For more than 30 years to get the proton FF the Coulomb factor for pointlike fermions has been applied. Therefore the proton FF, being obtained from a flat cross section divided by a steep increasing factor, has shown an apparent steep decrease, simulating the tail of a narrow resonance below threshold. Of course, assuming the FF are defined as additional factors with respect to the pointlike amplitude, one could take into account the pointlike Coulomb factor, but it seems unlikely to attach a physical meaning to the sharp decrease at threshold obtained in this way. To avoid this kind of ambiguity a better definition of FF in the time-like region might be proposed.

It has also been argued [107] that for the proton FF at threshold verify the identity  $G_E^p(4M_p^2) = G_M^p(4M_p^2) = 1$ , as achieved if the flat cross section is extrapolated down to the threshold and the divergent factor  $\pi\alpha/\beta$  is applied. After all such a result should not be so unexpected, since at threshold the overlap between  $\bar{p}$  and  $p$  wave function looks like the overlap of initial and final proton wave function in the case of electron proton scattering at a vanishing electron energy.

Coming back to the case of neutral baryon pair production, the fact that the cross section  $e^+e^- \rightarrow \Lambda\bar{\Lambda}$  is non zero at threshold strongly suggests that it is due to an unexpected Coulomb interaction at the quark level! This is surprising, since Coulomb interaction is a long range one, while strong interactions have a short range. As a consequence it was assumed until now that on a short time scale the hadron pair is created and after, on a much longer time scale, the Coulomb interaction takes over. To evaluate the expected cross section at threshold at the quark level a naive prediction (formulated some years ago [107]) would be that this cross section scales as the sum of the valence quarks charge squared, namely:

$$\sigma(4M_\Lambda^2) = \sigma(4M_p^2) \times \left(\frac{M_p}{M_\Lambda}\right)^2 \times \frac{Q_u^2 + Q_d^2 + Q_s^2}{Q_u^2 + Q_u^2 + Q_d^2} = 400 \text{ pb},$$

where  $Q_q$  is the charge of the quark  $q$ . Such expectation would be consistent with  $G_E^p(4M_p^2) = G_M^p(4M_p^2) = 1$  in the proton case, since  $Q_u^2 + Q_u^2 + Q_d^2 = 1$ . Surprisingly enough this very naive prediction is in good agreement with the  $e^+e^- \rightarrow \Lambda\bar{\Lambda}$  experimental result.

However this Coulomb contribution for neutral baryon pair production should vanish soon as the c.m. energy increased, somewhat in agreement with the aforementioned expectation as well as with the already mentioned *BABAR* cross section  $\sigma = 200 \pm 60 \pm 20$  pb, which is an average value from threshold up to  $W = 2270$  MeV [97]. Such a behaviour can be reproduced, if attractive and repulsive Coulomb factors both are taken into account with their proper sign in the amplitude, namely:

$$\mathcal{R}_{\text{eff}} = \left[ \frac{1}{\sqrt{\exp(\pi\alpha_{\text{eff}}/\tilde{\beta}) - 1}} - \frac{1}{\sqrt{1 - \exp(-\pi\alpha_{\text{eff}}/\tilde{\beta})}} \right]^2.$$

In this way, depending on  $\alpha_{\text{eff}}$ , as anticipated, since the hadron is neutral, they cancel each other except close to the threshold, producing a cusp in the cross section. Of course a further strong interaction contribution has to be included, which should behaves like:  $\beta \times G(W^2)$ , where  $G(W^2)$  should take into account the tails of resonances below threshold and asymptotically should scale like  $G(W^2) \propto W^{-10}$ . If Coulomb interaction is limited to a cusp it might be meaningful to disentangle the two contributions.

To trust all these speculations, confirmations are very welcome. More measurements will be needed in a range just above threshold to check this cusp behaviour and to check

if indeed  $\alpha \ll \alpha_{\text{eff}} \ll \alpha_s$ , assuming the model is meaningful. Furthermore, to establish a theory, a measurement of other hyperon cross sections at their own threshold will be needed too. Assuming the other charged and neutral hyperons have a behaviour similar to  $e^+e^- \rightarrow p\bar{p}$  or  $e^+e^- \rightarrow \Lambda\bar{\Lambda}$ , a series of spikes and jumps is expected.

Such that, the cross sections near thresholds have been measured by BESIII for other baryon pairs, for examples singly-stranged  $\Sigma^+\bar{\Sigma}^-$ ,  $\Sigma^-\bar{\Sigma}^+$  [108] and  $\Sigma^0\bar{\Sigma}^0$  [109] as shown in Fig. 15, doubly-stranged  $\Xi^-\bar{\Xi}^+$  [110] and  $\Xi^0\bar{\Xi}^0$  [111] as shown in Fig. 21.

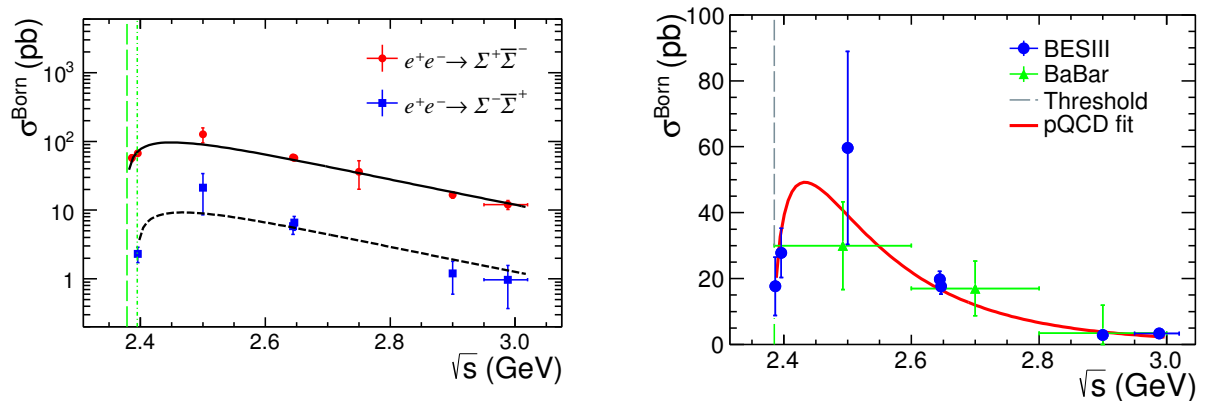


Figure 15: Left: the cross section lineshapes for  $e^+e^- \rightarrow \Sigma^+\bar{\Sigma}^-$  reactions (circles) and  $e^+e^- \rightarrow \Sigma^-\bar{\Sigma}^+$  (squares) [108]. The solid and dashed smooth lines are the pQCD fits. The vertical lines denoted their production thresholds. Right: Comparison plot of the cross sections for  $e^+e^- \rightarrow \Sigma^0\bar{\Sigma}^0$  reaction. The triangles in green are results from BaBar [97]. The solid line in red shows the pQCD fit.

Figure 16 shows the cross section lineshapes for a variety of baryon-antibaryon pairs have been measured so far [112]. They all seem to share the common feature with a plateau starting from the baryon-pair production threshold, though for some channels ideally more statistics are needed.

## 7 Hyperon form factors

In the time-like region ( $q^2 > 4m_B^2 > 0$ ,  $B$  refers to baryon), the form factors  $G_E(q)$  and  $G_M(q)$  are complex functions,  $G_E(q) = |G_E(q)|e^{i\Phi_E}$  and  $G_M(q) = |G_M(q)|e^{i\Phi_M}$  with a relative phase  $\phi = \Delta\Phi = \Phi_M - \Phi_E$ . The effective form factor, as defined for spin  $\frac{1}{2}$  baryons

$$|F|^2 = \frac{2\tau|G_M|^2 + |G_E|^2}{2\tau + 1} = \frac{2\tau}{(2\tau + 1)} \frac{3q^2\sigma}{4\pi\alpha^2\beta} \quad (22)$$

is obtained in the same way as for nucleons, *i.e.* from the energy dependence of the total cross section. Note that  $\tau = q^2/(4m^2)$  and  $\beta = 1 - 1/\tau$ . The electric and the magnetic

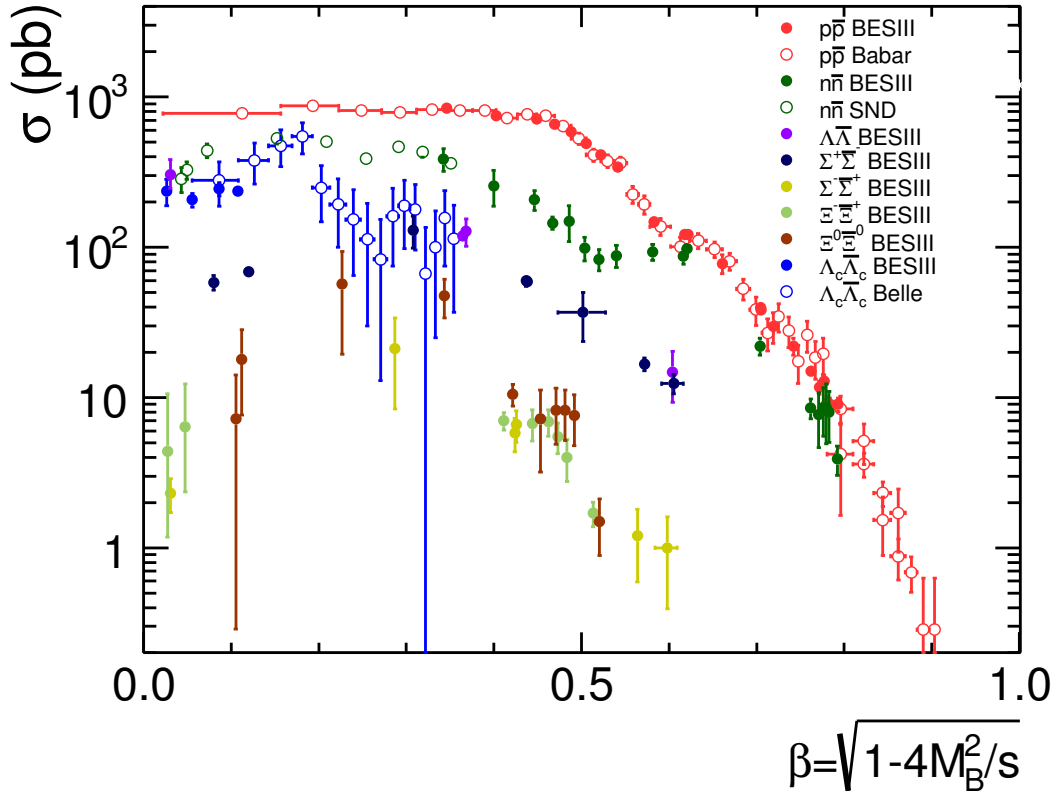


Figure 16: Cross sections of  $B\bar{B}$  pairs measured so far:  $p\bar{p}$  by BaBar [78, 79] and BESIII [85],  $n\bar{n}$  by SND [94, 95] and BESIII [93],  $\Lambda\bar{\Lambda}$  by BESIII [98],  $\Sigma^+\bar{\Sigma}^-/\Sigma^-\bar{\Sigma}^+$  by BESIII [108],  $\Xi^-\bar{\Xi}^+/\Xi^0\bar{\Xi}^0$  by BESIII [110, 111],  $\Lambda_c^+\bar{\Lambda}_c^-$  by Belle [113] and BESIII [114]. Plot is from [112].

form factors can then be expressed in the following way:

$$|G_M|^2 = \frac{2\tau + 1}{2\tau + R^2} |F|^2 \quad (23)$$

$$|G_E|^2 = R^2 \frac{2\tau + 1}{2\tau + R^2} |F|^2. \quad (24)$$

The ratio  $R = |G_E(q)|/|G_M(q)|$  can be extracted from the scattering angle of the outgoing baryon:

$$\frac{d\sigma}{d\cos\theta} = N_1((1 + \cos^2\theta)|G_M|^2 + \frac{1}{\tau}(1 - \cos^2\theta)|G_E|^2) \quad (25)$$

where  $N_1$  is an proportionality factor, constant in the angle and which depends on  $\alpha$ ,  $\beta$ , the Coloumb correction factor  $C$  and  $q$ .

Now consider production of spin  $\frac{1}{2}$  hyperon  $Y$ , produced in  $e^+e^- \rightarrow Y\bar{Y}$  and decaying into a spin  $\frac{1}{2}$  baryon and a pseudoscalar meson, for example  $e^+e^- \rightarrow \Lambda\bar{\Lambda}$ ,  $\Lambda \rightarrow p\pi^-$ . The reference system is defined in Fig. 17. The scattering plane is spanned by the  $e^+$  and the outgoing hyperon, *i.e.* its normal is defined by  $\hat{n} = \hat{e}_+ \times \hat{e}_\Lambda$  or equivalently, by the  $e^-$  and the outgoing antihyperon. The angle  $\theta$  is the scattering angle of the hyperon/antihyperon and the angle between the decay proton(antiproton) and  $\hat{n}$  is  $\theta_p(\theta_{\bar{p}})$ .

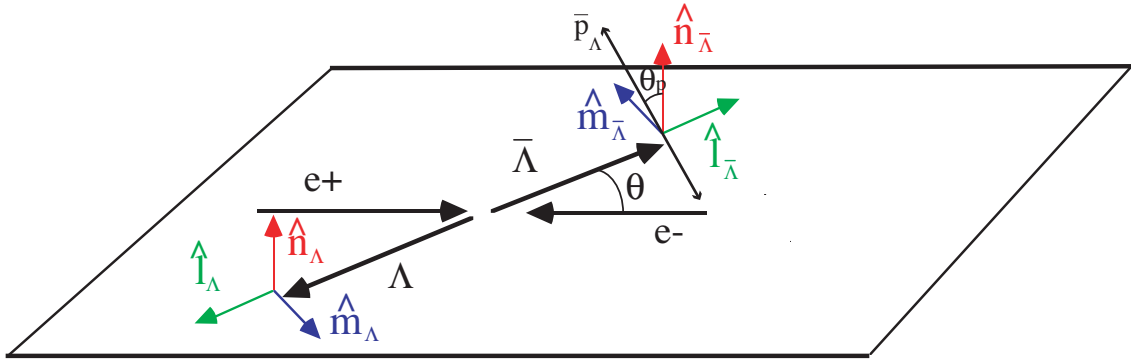


Figure 17: The coordinate system of the  $e^+e^- \rightarrow Y\bar{Y}$  process

The relative phase between the form factors has a polarizing effect on the final state hyperons. In Ref. [46], the polarization in terms of electromagnetic form factors  $G_E(q^2)$  and  $G_M(q^2)$  has been derived for unpolarised  $e^+$  and  $e^-$ , resulting in

$$P_n = -\frac{\sin 2\theta \text{Im}[G_E(q^2)G_M^*(q^2)]/\sqrt{\tau}}{(|G_E(q^2)|^2 \sin^2\theta)/\tau + |G_M(q^2)|^2(1 + \cos^2\theta)} = -\frac{\sin(2\theta) \sin(\phi)/\sqrt{\tau}}{\frac{R \sin^2(\theta)}{\tau} + \frac{1+\cos^2(\theta)}{R}} \quad (26)$$

where  $Im[G_E(q^2)G_M^*(q^2)] = |G_E(q^2)||G_M(q^2)| \sin \phi$  and  $R = |G_E(q^2)|/|G_M(q^2)|$ .  $\phi$  is the relative phase between the electric and the magnetic form factor and  $\tau = q^2/(4m_Y^2)$ . Thus, a measurement of the polarization determines the modulus of  $\sin \phi$ . From Eq. 26 it is clear that the polarization strongly depends on the scattering angle  $\theta$ . This has to be taken into account when extracting the phase.

In a similar way, the real part of the  $G_E G_M^*$ ,  $Re[G_E(q^2)G_M^*(q^2)] = |G_E(q^2)||G_M(q^2)| \cos \phi$  can be obtained from the correlation of the  $\Lambda$  and  $\bar{\Lambda}$  spins in the  $\hat{m}$  and  $\hat{l}$  directions [46]:

$$C_{lm} = \frac{\sin 2\theta Re[G_E(q^2)G_M^*(q^2)]/\sqrt{\tau}}{(|G_E(q^2)|^2 \sin^2 \theta)/\tau + |G_M(q^2)|^2(1 + \cos^2 \theta)} \quad (27)$$

Thus, by measuring the effective form factor, the angular distribution of the hyperon and the polarisation and  $\Lambda\bar{\Lambda}$  spin correlations, the time-like form factors can be fully determined.

## 7.1 Existing data and theoretical predictions

Very few measurements have been performed on  $e^+e^- \rightarrow Y\bar{Y}$  channels. The DM2 collaboration measured the  $e^+e^- \rightarrow \Lambda\bar{\Lambda}$  cross section at a CM energy 2.386 GeV [115] and found it to be  $\sigma(e^+e^- \rightarrow \Lambda\bar{\Lambda}) = 100_{-35}^{+65} pb$ .

BABAR used ISR data at a  $e^+e^-$  CM energy of 10.58 GeV to extract the cross section/effective form factor 12 points in  $M(\Lambda\bar{\Lambda})$  [97]. Their total event sample consisted of only  $\approx 200$  events and the relative error in each point was large (typically  $> 30\%$ ). The ratio was extracted in two different energy ranges:

- $|G_E/G_M| = 1.73_{-0.57}^{+0.99}$  for  $2.23 < q < 2.4$  GeV
- $|G_E/G_M| = 0.71_{-0.71}^{+0.66}$  for  $2.24 < q < 2.6$  GeV

They also calculated the phase, but integrated over all scattering angles and all energies, and assuming a ratio of  $|G_E/G_M| = 1$ . Consequently the result was inconclusive:  $-0.76 < \sin \phi < 0.98$ .

On the theoretical side, Czyz, Grzelinska and Kühn adopted in Ref. [116] a model from Körner and Kuroda [117] which predicts real form factors, *i.e.* zero phase and unpolarised hyperons. Calculations have been made by Bartos *et al.* [118] of the moduli of the Sachs form factors of  $\Lambda$ ,  $\Sigma$  and  $\Xi$  based on the Unitary and Analytic model [119]. There are recent predictions by the same group of vector- and tensor polarisations of nucleons [120].

- more precise data on hyperon form factors, *i.e.* the effective form factor and the ratio  $R$ , or
- lepton decay widths for the ground state, the first excitation and the second excitation of  $\rho$ ,  $\omega$  and  $\phi$  mesons, from which one could determine the universal vector meson coupling constants.

More experimental data will therefore stimulate the theoretical activity of the field.

## 7.2 Hyperon form factors with BESIII

### 7.2.1 The $\Lambda$ hyperon

Based on test run data at four energies, the  $\Lambda$  effective form factor was extracted by BESIII [98], as shown in Fig. 18.

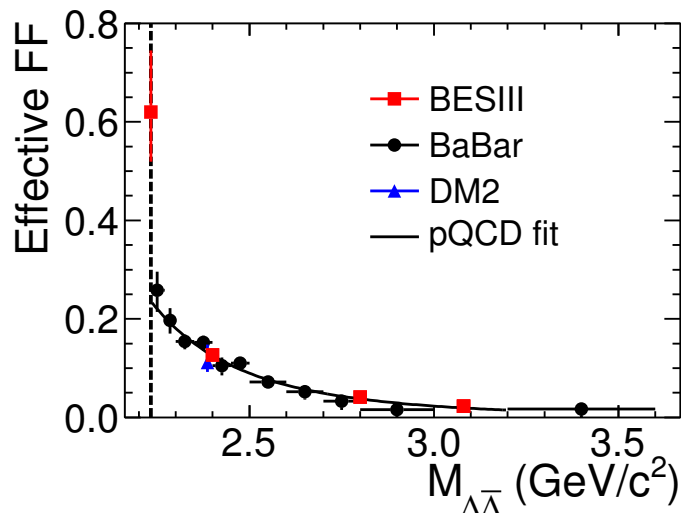


Figure 18:  $\Lambda$  effective form factor.

According to the optical theorem, there is a nonzero relative phase between  $G_E$  and  $G_M$ . At  $M_{\Lambda\bar{\Lambda}} = 2.396$  GeV, where the largest  $\Lambda\bar{\Lambda}$  sample of 555 events from  $66.9 \text{ pb}^{-1}$  data was accumulated later, a multidimensional analysis was used to make a full determination of the  $\Lambda$  electromagnetic form factors for the first time for any baryon; the relative phase difference is  $\Delta\Phi = 37^\circ \pm 12^\circ \pm 6^\circ$  [121] with the input parameter  $\alpha_\Lambda = 0.750 \pm 0.010$  measured from  $J/\psi$  decays [122]. The improved determination of  $\alpha_\Lambda$  also has profound implications for the baryon spectrum, since fits to such observables by theoretical models are a crucial element in determining the light baryon resonance spectrum, which provides a point of comparison for theoretical approaches [123]. The  $|G_E/G_M|$  ratio was determined to be  $R = 0.96 \pm 0.14(\text{stat.}) \pm 0.02(\text{sys.})$  and the effective form factor

at  $M_{\Lambda\bar{\Lambda}} = 2.396$  GeV was determined to be  $|G_{eff}| = 0.123 \pm 0.003(\text{stat.}) \pm 0.003(\text{sys.})$ . The  $\Lambda$  angular distribution and the polarization as a function of the scattering angle are shown in Fig. 19(a) and (b) [121], respectively. This first complete measurement of the hyperon electromagnetic form factor is a milestone in the study of hyperon structure.

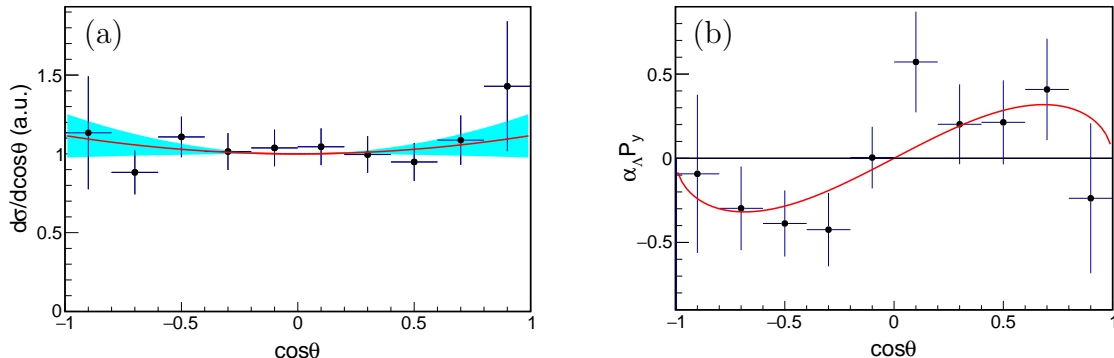


Figure 19: (a) The acceptance corrected  $\Lambda$  scattering angle distribution for  $e^+e^- \rightarrow \Lambda\bar{\Lambda}$  at  $M_{\Lambda\bar{\Lambda}} = 2.396$  GeV. (b) The product of the  $\Lambda$  decay parameter  $\alpha_\Lambda$  and  $\Lambda$  polarization  $P_y$  as a function of the scattering angle.

## 7.2.2 The $\Sigma$ hyperons

BESIII studied the processes  $e^+e^- \rightarrow \Sigma^\pm\bar{\Sigma}^\mp$  and  $e^+e^- \rightarrow \Sigma^0\bar{\Sigma}^0$  reactions from 2.3864 to 3.0200 GeV and determined the timelike EMFFs of  $\Sigma$  hyperons with high precision [108, 109]. Born cross sections of  $\Sigma^\pm\bar{\Sigma}^\mp$  pair productions, effective form factors  $|G_{eff}|$  of  $\Sigma^+$  and  $\Sigma^-$ , the ratios of  $\Sigma^+$  electric and magnetic FFs  $|G_E/G_M|$ , were reported [108]. For c.m.energies near threshold, a novel method was used to reconstruct the neutral channel  $e^+e^- \rightarrow \Sigma^0\bar{\Sigma}^0$  whereas a single-hyperon-tag method was applied for c.m. energies between 2.5000 and 3.0200 GeV. Born cross sections are measured with significantly improved precision [109] to those of BaBar [97]. The  $|G_{eff}|$  of  $\Sigma^0$  was also reported.

Near production threshold of  $\Sigma^\pm\bar{\Sigma}^\mp$  pairs, the cross section were observed to be  $(58.2 \pm 5.9_{-2.6}^{+2.8})$  pb and  $(2.3 \pm 0.5 \pm 0.3)$  pb, which disagrees with the pointlike expectations close to threshold of  $848(m_p/m_B)^2$  pb. The cross section lineshapes presented in Fig. 15 for  $e^+e^- \rightarrow \Sigma^+\bar{\Sigma}^-$  and  $e^+e^- \rightarrow \Sigma^-\bar{\Sigma}^+$  are well-described by pQCD-motivated functions. The ratio of the  $\sigma^{\text{Born}}(e^+e^- \rightarrow \Sigma^+\bar{\Sigma}^-)$  to  $\sigma^{\text{Born}}(e^+e^- \rightarrow \Sigma^-\bar{\Sigma}^+)$  was found to be  $9.7 \pm 1.3$ , which is inconsistent with predictions. The EFF is proportional to the square root of the cross section, and the observed ratio of  $|G_{eff}^{\Sigma^+}(s)|/|G_{eff}^{\Sigma^-}(s)|$  was found to be consistent with 3, which is the ratio of the incoherent sum of the squared charges of valence quarks in  $\Sigma^+$  and  $\Sigma^-$  baryons,  $\sum_q Q_q^2$ , with  $q = u, d, s$ . Furthermore, the EMFF

ratio  $|G_E(s)/G_M(s)|$  of the  $\Sigma^+$  was reported through an angular analysis at three high-statistics energy points, 2.3960, 2.6444, and 2.6464 GeV for  $e^+e^- \rightarrow \Sigma^+\bar{\Sigma}^-$ . Based on the polar angular distribution of  $\Sigma^+$ , the ratio  $|G_E(s)/G_M(s)|$  of the  $\Sigma^+$  baryon was determined to be  $|G_E(s)/G_M(s)| = 1.83 \pm 0.26$  near threshold, which is significantly higher than 1 [108].

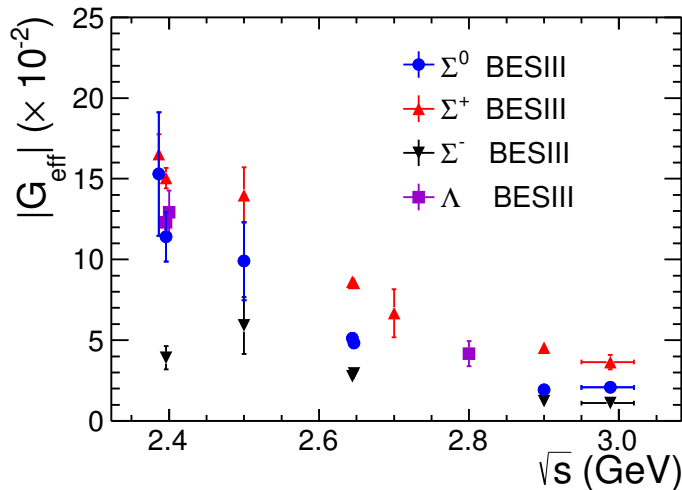


Figure 20: Effective form factors of hyperons measured at BESIII [108, 109, 98, 121].

### 7.2.3 The $\Xi$ hyperons

BESIII measured Born cross sections and EFFs for the processes  $e^+e^- \rightarrow \Xi^-\bar{\Xi}^+$  [110] and  $e^+e^- \rightarrow \Xi^0\bar{\Xi}^0$  [111] based on a single hyperon tag method using data collected at c.m. energies between 2.644 and 3.080 GeV. Figure 21 shows the measured Born cross sections and EFFs for the two processes.

## 8 Form factors of charmed baryon

Higher energy opens a windows for charmed baryon studies. Previously there were no sufficient data above charmed baryon production threshold, and therefore no form factor results were reported. The only measurement of cross section of the process  $e^+e^- \rightarrow \Lambda_c^+\bar{\Lambda}_c^-$  is from the Belle experiment, which measured the cross section using ISR technique [113], and reported a lineshape that implied the existence of a likely resonance, called the  $Y(4660)$ . Based on  $631.3 \text{ pb}^{-1}$  data collected in 2014 at four energy points  $\sqrt{s} = 4.5745, 4.5809, 4.5900$  and  $4.5995$  GeV, BESIII measured the  $\Lambda_c^+\bar{\Lambda}_c^-$  cross section with unprecedented precision [114]. The lowest energy point is only 1.6

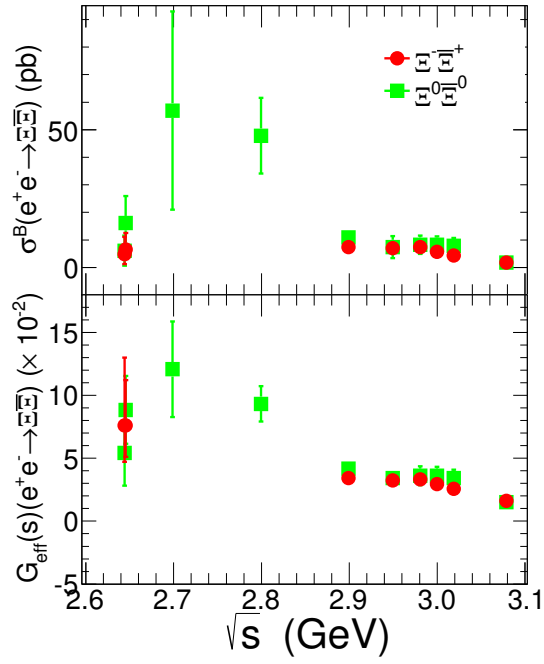


Figure 21: Born cross sections (**top**) and EFTs (**bottom**) of  $e^+e^- \rightarrow \Xi^- \bar{\Xi}^+$  and  $e^+e^- \rightarrow \Xi^0 \bar{\Xi}^0$  from 2.6 to 3.1 GeV.

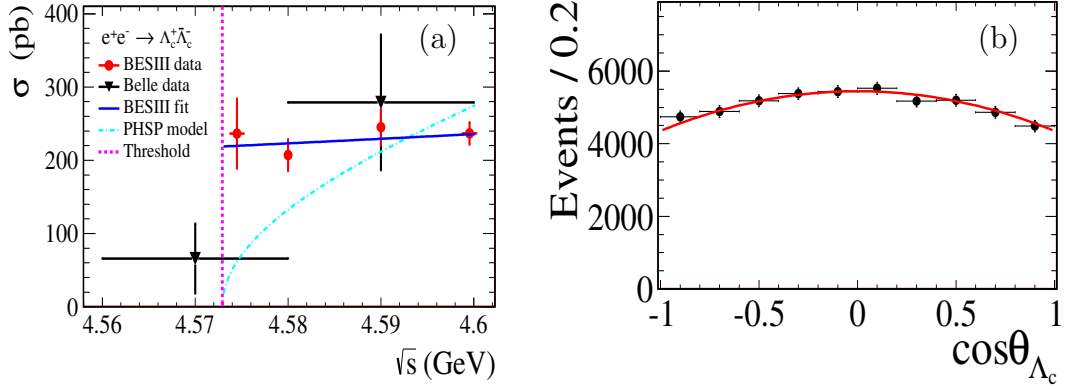


Figure 22: The Born cross section of  $e^+e^- \rightarrow \Lambda_c^+ \bar{\Lambda}_c^-$  obtained by BESIII and Belle (a). The angular distribution and corresponding fit results in data at  $\sqrt{s} = 4.5995$  GeV (b).

MeV above the  $\Lambda_c^+ \bar{\Lambda}_c^-$  threshold. At each of the energy points, ten Cabibbo-favored hadronic decay modes,  $\Lambda_c^+ \rightarrow pK^-\pi^+$ ,  $pK_S^0$ ,  $\Lambda\pi^+$ ,  $pK^-\pi^+\pi^0$ ,  $pK^0\pi^0$ ,  $\Lambda\pi^+\pi^0$ ,  $pK_S\pi^+\pi^-$ ,  $\Lambda\pi^+\pi^+\pi^-$ ,  $\Sigma^0\pi^+$ , and  $\Sigma^+\pi^+\pi^-$ , as well as the corresponding charge-conjugate modes were studied. The total Born cross section is obtained from the weighted average of the 20 individual measurements, and the results are shown in Fig. 22(a). Similar to the case for  $e^+e^- \rightarrow p\bar{p}$ , an abrupt rise in the cross-section just above threshold that is much steeper than phase-space expectations is discerned, which was not seen by Belle due to limitations of the ISR method. BESIII's measured cross section lineshape is different from Belle's, disfavoring a resonance like  $Y(4660)$  in the  $\Lambda_c^+ \bar{\Lambda}_c^-$  channel. The BESIII results have driven discussions in the theoretical literature [124].

The relatively larger samples at  $\sqrt{s} = 4.5745$  and  $4.5995$  GeV enabled studies of the polar angular distribution of  $\Lambda_c$  in the  $e^+e^-$  center-of-mass system. The shape function  $f(\theta) \propto (1 + \alpha_{\Lambda_c} \cos^2 \theta)$  is fitted to the combined data containing the yields of  $\Lambda_c^+$  and  $\bar{\Lambda}_c^-$  for all ten decay modes as shown in Fig. 22(b). The ratio between the electric and magnetic form factors  $|G_E/G_M|$  can be extracted using  $|G_E/G_M|^2(1 - \beta^2) = (1 - \alpha_{\Lambda_c})/(1 + \alpha_{\Lambda_c})$ . From these distributions, the ratios  $|G_E/G_M|$  of  $\Lambda_c^+$  have been extracted for the first time: they are  $1.14 \pm 0.14$  (stat.)  $\pm 0.07$  (sys.) and  $1.23 \pm 0.05$  (stat.)  $\pm 0.03$  (sys.) at  $\sqrt{s} = 4.5745$  and  $4.5995$  GeV, respectively.

At a future STCF with energy up to 7 GeV, it is natural to extend the studies to other charmed baryons including  $\Sigma_c$ ,  $\Xi_c$ ,  $\Omega_c$  and their excited states.

## 9 Summary

For a long time the overall uncertainties on two of the fundamental quantities  $\alpha(M_Z)$  and  $a_\mu$  had been dominated by the poor precision (15-20% accuracy) of the  $R$  values at the energies between 1 – 5 GeV. BESII reduced the uncertainty of  $R$  values in 2 – 5 GeV to a level of 6 – 7%, which helped a lot in the Standard Model fitting. Recently BESIII has reached a precision better than 3% in the continuum region. Nonetheless, with the improvement of measurement precision in other energy regions as well, especially in the region below 2 GeV, once again the uncertainty of  $R$  values in 2 – 5 GeV becomes a limiting factor. In view of the importance of accurate values of  $\alpha(M_Z)$  and  $a_\mu$  for the precision test of the SM, new measurements of  $R$  with a precision towards (1 ~ 3)% are strongly encouraged and called for at future STCF. Such a measurement is also important for the evaluation of the strong coupling constant  $\alpha_s$  and the charm quark mass.

It will be a very difficult task to measure  $R$  to a precision of a percent in the energy region of 2 – 5 GeV. A great effort has to be made to reduce the uncertainty in the detection efficiency for the hadronic events and luminosity measurement, and beam associated background and initial state radiative correction also have to be examined carefully.

Hadron production and hadron structure are yet to be further studied, preferably with high-quality and large-statistics data at a future STCF. Some important topics, like form factor measurement, production threshold behavior study, fragmentation function investigation, etc., are essential to understand the strong interaction ultimately.

## References

- [1] Q. Luo and D. Xu, Progress on Preliminary Conceptual Study of HIEPA, a Super Tau-Charm Factory in China. 9th International Particle Accelerator Conference (IPAC 2018), Vancouver, Canada, April 29-May 4, 2018.
- [2] A. Y. Barnyakov, The project of the Super Charm-Tau Factory in Novosibirsk. J. Phys. Conf. Ser. 2020; **1561**: 012004.
- [3] S. L. Glashow, Nucl.. Phys. 22 (1961) 579
- [4] S. Weinberg, Phys. Rev. Lett. 19 (1967) 124
- [5] N. Cabibbo and R. Catto, Phys. Rev. 124 (1961)1577
- [6] A. Keshavarzi, D. Nomura and T. Teubner, Phys. Rev. D97, 114025 (2018)
- [7] J. Bailey et al., Phys. Lett. B 68 (1977),

- [8] F.J.M. and E. Picasso, *Ann. Rev. Nucl. Sci.* 29 (1979) 243
- [9] F.J.M. Farley, *Z. Phys. C* 56 (1992) S88
- [10] G.W. Bennett et al. (Muon  $g-2$  Collaboration), *Phys.Rev.Lett.* 92 (2004) 161802, *Phys. Rev. D* 73, 072003 (2006).
- [11] D.J. Broadhurst, et al., *Phys. Lett. B* 298 (1993) 445
- [12] T. Kinoshita *Phys. Rev. D* 47 (1993) 5013
- [13] T. Kinoshita and W.J. Marciano, in 'Quantum Electrodynamics', ed. T. Kinoshita, World Scientific, Singapore, 1990, pp. 419-478
- [14] P. Mery, et al., *Z. Phys. C* 46 (1990) 229
- [15] W. Bernreuther, *Z. Phys. C* 56 (1992) S97
- [16] D. H. Brown et al., *Phys. Rev. D* 54 (1996) 3237, A. Czarnecki, et al., 'Electroweak corrections to the muon anomalous magnetic moment', hep-ph 9512369
- [17] T. Aoyama, N. Asmussen, M. Benayoun *et al.*, [Phys. Rep. \*\*887\*\*, 1 \(2020\)](#).
- [18] B. Abi *et al.* (Muon  $g - 2$  Collaboration), [Phys. Rev. Lett. \*\*126\*\*, 141801 \(2021\)](#).
- [19] S. G. Gorishny et. al., *Phys. Lett. B*259 (1991) 144 R. Marshall, *Z. Phys. C* 43 (1988) 595
- [20] P.A. Zyla et al. (Particle Data Group), *Prog. Theor. Exp. Phys.* 2020, 083C01 (2020) and 2021 update
- [21]  $\mu\pi$  group: F. Ceradini et al., *Phys. Lett. B* 47 (1973) 80;  $\gamma\gamma$  group: C. Bacci et al., *ibid.* B 44 (1973) 533; Boson group: B. Batoli et al., *Phys. Rev. D* 6 (1972) 2374; BCF group: M. Bernardini et al., *Phys. Lett. B* 51 (1974) 200
- [22] G. Cosme et al., *Phys. Lett. B* 40 (1972) 685 and references herein
- [23] M. Kurdadze et al., *Phys. Lett. B* 42 (1972) 515
- [24] Litke et al., *Phys. Rev. Lett.* 30 (1973) 1189 *Phys. Rev. Lett.* 30 (1973) 1349
- [25] BES Collaboration, J. Z. Bai et al., *Phys. Rev. Lett.* 84, 594 (2000); BES Collaboration, J. Z. Bai et al., *Phys. Rev. Lett.* 88, 101802 (2002)
- [26] A. E. Blinov et al., *Z.Phys. C*70 (1996) 31
- [27] CLEO Collaboration, D. Besson et al., *Phys. Rev. D*76 (2007) 072008

- [28] V. V. Anashin *et al.* (KEDR Collaboration), [Phys. Lett. B \*\*753\*\*, 533 \(2016\)](#).
- [29] V. V. Anashin *et al.* (KEDR Collaboration), [Phys. Lett. B \*\*770\*\*, 174 \(2017\)](#).
- [30] V. V. Anashin *et al.* (KEDR Collaboration), [Phys. Lett. B \*\*788\*\*, 42 \(2019\)](#).
- [31] M. Ablikim *et al.* (BESIII Collaboration), [Phys. Rev. Lett. \*\*128\*\*, 062004 \(2022\)](#).
- [32] R. Brandelik *et al.* DASP Collaboration, *Phys. Lett. B* **76** (1978) 361
- [33] J. L. Siegrist *et al.* Mark I Collaboration, *Phys. Rev. D* **26** (1982) 969
- [34] J. Burmeister *et al.* PLUTO Collaboration, *Phys. Lett. B* **66** (1977) 395
- [35] M. Ablikim *et al.*, BES Collaboration, *Phys. Lett. B* **660**, 315 (2008)
- [36] D. Cronin-Hennessy *et al.*, CLEO Collaboration, *Phys. Rev. D* **80**, 072001 (2009)
- [37] G. Pakhlova, Belle Collaboration, International Workshop on  $e^+e^-$  from Phi to Psi, 13-16 October, 2009, Beijing, China
- [38] M. Ablikim *et al.*, BES Collaboration, *Phys. Lett. B* **677** (2009) 239
- [39] Diogo Boito and Vicent Mateu, [JHEP \*\*03\*\*, 094 \(2020\)](#).
- [40] J.H.Kühn and M.Steinhauser, *Nucl. Phys. B* **619**, 588 (2001)
- [41] J.Peñarrocha and K.Schilcher, *Phys. Lett B* **515**, 291 (2001)
- [42] V.A. Khoze and W. Ochs, *Int. J. Mod. Phys. A* **12**, 2949 (1997).
- [43] Ya.I. Azimov, Yu.L. Dokshitzer, V.A. Khoze, and S.I. Troyan, *Phys. Lett. B* **165**, 147 (1985); *Z. Phys. C* **27**, 65 (1985)
- [44] J.Z. Bai, BES Collaboration, *Phys. Rev. D* **69**, 072002 (2004)
- [45] M. Ablikim *et al.*, BES Collaboration, *Phys. Lett. B* **630** (2005) 14
- [46] A. Z. Dubnickova, S. Dubnicka and M.P. Rekaló, *Nuovo Cim. A* **109** (1996) 241.
- [47] D.B. Lichtenberg and J.G. Wills, *Phys. Rev. Lett.* **35** 1055 (1975).
- [48] Dian-Yong Chen *et al.*, *Eur. Phys. J. C* **72**, 2008 (2012).
- [49] B. Aubert *et al.* (BABAR Collaboration), *Phys. Rev. D* **74**, 091103(R) (2006); **76**, 012008 (2007).
- [50] J. P. Lees *et al.* (BABAR Collaboration), *Phys. Rev. D* **86**, 012008 (2012).

- [51] C. P. Shen *et al.* (Belle Collaboration), Phys. Rev. D **80**, 031101(R) (2009).
- [52] M. Ablikim *et al.* (BES Collaboration), Phys. Rev. Lett. **100**, 102003 (2008).
- [53] M. Ablikim *et al.* (BESIII Collaboration), Phys. Rev. D **91**, 052017 (2015).
- [54] M. Ablikim *et al.* (BESIII Collaboration), Phys. Rev. D **99**, 012014 (2019).
- [55] T. Barnes, N. Black, and P. R. Page, Phys. Rev. D **68**, 054014 (2003).
- [56] G. J. Ding and M. L. Yan, Phys. Lett. B **657**, 49 (2007); Q. Li, L. C. Gui, M. S. Liu, Q. F. Lv, and X. H. Zhong, arXiv: 2004.05786.
- [57] G. J. Ding and M. L. Yan, Phys. Lett. B **650**, 390 (2007).
- [58] P. R. Page, E. S. Swanson, and A. P. Szczepaniak, Phys. Rev. D **59**, 034016 (1999).
- [59] Z. G. Wang, Nucl. Phys. A **791**, 106 (2007).
- [60] H. X. Chen, X. Liu, A. Hosaka, and S. L. Zhu, Phys. Rev. D **78**, 034012 (2008).
- [61] N. V. Drenska, R. Faccini, and A. D. Polosa, Phys. Lett. B **669**, 160 (2008).
- [62] H. W. Ke and X. Q. Li, Phys. Rev. D **99**, 036014 (2019).
- [63] S. S. Agaev, K. Azizi, and H. Sundu, Phys. Rev. D **101**, 074012 (2020).
- [64] E. Klempt and A. Zaitsev, Phys. Rep. **454**, 1 (2007).
- [65] C. F. Qiao, Phys. Lett. B **639**, 263 (2006).
- [66] Y. B. Dong *et al.*, Phys. Rev. D **96**, 074027 (2017).
- [67] Y. L. Yang, D. Y. Chen, and Z. Lu, Phys. Rev. D **100**, 073007 (2019).
- [68] S. L. Zhu, Int. J. Mod. Phys. E **17**, 283 (2008).
- [69] A. M. Torres, K. P. Khemchandani, L. S. Geng, M. Napsuciale, and E. Oset, Phys. Rev. D **78**, 074031 (2008).
- [70] M. Ablikim *et al.* (BESIII Collaboration), Phys. Rev. D **99**, 032001 (2019).
- [71] M. Ablikim *et al.* (BESIII Collaboration), Phys. Rev. D **104**, 092014 (2021).
- [72] M. Ablikim *et al.* (BESIII Collaboration), Phys. Rev. Lett. **124**, 112001 (2020).
- [73] M. Ablikim *et al.* (BESIII Collaboration), Phys. Rev. D **100**, 032009 (2019).

- [74] M. Ablikim *et al.* (BESIII Collaboration), Phys. Rev. D **104**, 032007 (2021).
- [75] M. Ablikim *et al.* (BESIII Collaboration), Phys. Rev. D **102**, 012008 (2020).
- [76] M. Ablikim *et al.* (BESIII Collaboration), Phys. Lett. B **813**, 136059 (2021).
- [77] Quarks and leptons: an introductory course in modern particle physics, by Francis Halzen and Alan D. Martin
- [78] Lees JP, Poireau V and Tisserand V *et al.* [BaBar Collaboration]. Study of  $e^+e^- \rightarrow p\bar{p}$  via initial-state radiation at BABAR. Phys. Rev. D 2013; **87**: 092005.
- [79] Lees JP, Poireau V and Tisserand V *et al.* [BaBar Collaboration]. Measurement of the  $e^+e^- \rightarrow p\bar{p}$  cross section in the energy range from 3.0 to 6.5 GeV. Phys. Rev. D 2013; **88**: 072009.
- [80] Bardin G, Burgun G, Calabrese R, Capon G, Carlin R (1994) *et al.* Nucl. Phys. B **411** 3-32
- [81] Antonelli A *et al* 1998 Nucl. Phys. B **517** 3
- [82] Zichichi A, Berman S M, Cabibbo N and Gatto R 1962 *Nuovo Cimento* **24** 170
- [83] Tzara C 1970 Nucl. Phys. B **18** 216-252
- [84] Ablikim M, Achasov MN and Ai XC *et al.* [BESIII Collaboration]. Measurement of the proton form factor by studying  $e^+e^- \rightarrow p\bar{p}$ . Phys. Rev. D 2015; **91**: 112004.
- [85] Ablikim M, Achasov MN and Adlarson P *et al.* [BESIII Collaboration]. Measurement of proton electromagnetic form factors in  $e^+e^- \rightarrow p\bar{p}$  in the energy region 2.00 - 3.08 GeV. Phys. Rev. Lett. 2020; **124**: 042001.
- [86] Ablikim M, Achasov MN and Adlarson P *et al.* [BESIII Collaboration]. Study of the process  $e^+e^- \rightarrow p\bar{p}$  via initial state radiation at BESIII. Phys. Rev. D 2019; **99**: 092002.
- [87] Ablikim M, Achasov MN and Adlarson P *et al.* [BESIII Collaboration]. Measurement of proton electromagnetic form factors in the time-like region using initial state radiation at BESIII. Phys. Lett. B 2021; **817**: 136328.
- [88] Akhmetshin RR, Amirkhanov AN and Anisenkov AV *et al.* [CMD-3 Collaboration]. Observation of a fine structure in  $e^+e^- \rightarrow$  hadrons production at the nucleon-antinucleon threshold. Phys. Lett. B 2019; **794**: 64-68.

- [89] Adamuscin C, Dubnicka S and Dubnickova AZ *et al.* A unitary and analytic model of nucleon EM structure, the puzzle of JLab proton polarization data and new insight into the proton charge distribution. *Prog. in Parti. and Nucl. Phys.* 2005; **55**: 228-241.
- [90] Dubnickova AZ and Dubnicka S. Proton em form factors data are in disagreement with new  $\sigma_{tot}(e^+e^- \rightarrow p\bar{p})$  measurements. arXiv:2010.15872 [hep-ph] (2020).
- [91] Dalkarov OD, Khakhulin PA and Voronin AY. On the electromagnetic form factors of hadrons in the time-like region near threshold. *Nucl. Phys. A* 2010; **833**: 104-118.
- [92] Bianconi A and Tomasi-Gustafsson E. Periodic interference structures in the time-like proton form factor. *Phys. Rev. Lett.* 2015; **114**: 232301.
- [93] Ablikim M, Achasov MN and Adlarson P *et al.* [BESIII Collaboration]. Oscillating features in the electromagnetic structure of the neutron. *Nat. Phys.* 2021; **17**: 1200.
- [94] Achasov MN, Barnyakov AY and Beloborodov KI *et al.* [SND Collaboration]. Study of the process  $e^+e^- \rightarrow n\bar{n}$  at the VEPP-2000  $e^+e^-$  collider with the SND detector. *Phys. Rev. D* 2014; **90**: 112007.
- [95] Druzhinin VP and Serebnyakov SI. Measurement of the  $e^+e^- \rightarrow n\bar{n}$  cross section with the SND detector at the VEPP-2000 collider. *EPJ Web Conf.* 2019; **212**: 07007.
- [96] Bisello D, Busetto G and Castro A *et al.* [DM2 Collaboration]. Baryon pairs production in  $e^+e^-$  annihilation at  $\sqrt{s} = 2.4$  GeV. *Z. Phys. C* 1990; **48**: 23-28.
- [97] Aubert B, Bona M and Boutigny D *et al.* [BABAR Collaboration]. Study of  $e^+e^- \rightarrow \Lambda\bar{\Lambda}, \Lambda\bar{\Sigma}^0, \Sigma^0\bar{\Sigma}^0$  using initial state radiation with BABAR. *Phys. Rev. D* 2007; **76**: 092006.
- [98] Ablikim, M.; Achasov, M. N.; Ahmed, S.; et al. Observation of a cross-section enhancement near mass threshold in  $e^+e^- \rightarrow \Lambda\bar{\Lambda}$ . *Phys. Rev. D* **2018**, *97*, 032013.
- [99] El-Bennich B, Lacombe M and Loiseau B *et al.* Paris  $N\bar{N}$  potential constrained by recent antiprotonic-atom data and  $\bar{n}p$  total cross sections. *Phys. Rev. C* 2009; **79**: 054001.
- [100] Xiao LY, Weng XZ and Zhong XH *et al.* A possible explanation of the threshold enhancement in the process  $e^+e^- \rightarrow \Lambda\bar{\Lambda}$ . *Chin. Phys. C* 2019; **43**: 113105.
- [101] Baldini R, Pacetti S and Zallo A *et al.* Unexpected features of  $e^+e^- \rightarrow p\bar{p}$  and  $e^+e^- \rightarrow \Lambda\bar{\Lambda}$  cross-sections near threshold. *Eur. Phys. J. A* 2009; **39**: 315-321.

- [102] Baldini Ferroli R, Pacetti S and Zallo A. No Sommerfeld resummation factor in  $e^+e^- \rightarrow p\bar{p}$ ? Eur. Phys. J. A 2012; **48**: 33.
- [103] Zou BS and Chiang HC. One-pion-exchange final-state interaction and the  $p\bar{p}$  near threshold enhancement in  $J/\psi \rightarrow \gamma p\bar{p}$  decays. Phys. Rev. D 2004; **69**: 034004.
- [104] Haidenbauer J, Hammer HW and Meißner UG *et al.* On the strong energy dependence of the  $e^+e^- \leftrightarrow p\bar{p}$  amplitude near threshold. Phys. Lett. B 2006; **643**: 29-32.
- [105] Haidenbauer J and Meißner UG. The electromagnetic form factors of the  $\Lambda$  in the timelike region. Phys. Lett. B 2016; **761**: 456-461.
- [106] A. D. Sakharov, Zh. Eksp. Teor. Fiz. **18**, 631 (1948) [Sov. Phys. Usp. 34, 375 (1991)]; A. Sommerfeld, Atombau und Spektrallinien (Vieweg, Braunschweig, 1944), Vol. 2, p.130; J. Schwinger, Particles, Sources, and Fields, Vol. III, p. 80.
- [107] R. Baldini, S. Pacetti, A. Zallo and A. Zichichi, Eur. Phys. J. A **39** (2009) 315 [arXiv:0711.1725 [hep-ph]].
- [108] Ablikim, M.; Achasov, M.N.; Adlarson, P.; et al. Measurements of  $\Sigma^+$  and  $\Sigma^-$  timelike electromagnetic form factors for center-of-mass energies from 2.3864 to 3.0200 GeV. *Phys. Lett. B* **2021**, *814*, 136110.
- [109] Ablikim, M.; Achasov, M.N.; Adlarson, P.; et al. Measurement of the  $e^+e^- \rightarrow \Sigma^0\bar{\Sigma}^0$  cross sections at center-of-mass energies from 2.3864 to 3.0200 GeV. arXiv:2110.04510v1.
- [110] Ablikim M, Achasov MN and Adlarson P *et al.* [BESIII Collaboration]. Measurement of cross section for  $e^+e^- \rightarrow \Xi^-\bar{\Xi}^+$  near threshold at BESIII. Phys. Rev. D 2021; **103**: 012005.
- [111] Ablikim M, Achasov MN and Adlarson P *et al.* [BESIII Collaboration]. Measurement of cross section for  $e^+e^- \rightarrow \Xi^0\bar{\Xi}^0$  near threshold. Phys. Lett. B 2021; **820**: 136557.
- [112] Huang, G.S.; Baldini Ferroli, R. Probing the internal structure of baryons. *Natl. Sci. Rev.* **2021**, *8*, nwab187.
- [113] Pakhlova G, Adachi I and Aihara H *et al.* [Belle Collaboration]. Observation of a Near-Threshold Enhancement in the  $e^+e^- \rightarrow \Lambda_c^+\Lambda_c^-$  Cross Section Using Initial-State Radiation. Phys. Rev. Lett. 2008; **101**: 172001.

- [114] Ablikim M, Achasov MN and Ahmed S *et al.* [BESIII Collaboration]. Precision measurement of the  $e^+e^- \rightarrow \Lambda_c^+\bar{\Lambda}_c^-$  cross section near threshold. *Phys. Rev. Lett.* 2018; **120**: 132001.
- [115] D. Bisello *et al.*, *Z. Phys. C* 48 (1990) 23.
- [116] H. Czyz, A. Grzelinska and J.H. Kühn, *Phys. Rev. D* **75** (2007) 074026.
- [117] J. G. Körner and M. Kuroda, *Phys. Rev. D.* 16 (1977) 2165.
- [118] E. Bartos, A. Z. Dubnickova and S. Dubnicka, *Nucl. Phys. B (Proc. Suppl.)* 219-220 (2011) 166.
- [119] S. Dubnicka and A. Z. Dubnickova, *Acta Phys. Slov.* 60 (2010) 1.
- [120] S. Dubnicka *et al.*, talk at the EPS HEP Conference in Stockholm, Sweden (2013).
- [121] Ablikim, M.; Achasov, M.N.; Adlarson, P.; et al. Complete measurement of the  $\Lambda$  electromagnetic form factors. *Phys. Rev. Lett.* **2019**, *123*, 122003.
- [122] Ablikim M, Achasov MN and Ahmed S *et al.* [BESIII Collaboration]. Polarization and Entanglement in Baryon-Antibaryon Pair Production in Electron-Positron Annihilation. *Nature Physics* 2019; **15**: 631-634.
- [123] Ireland DG, Döring M and Glazier DI *et al.* Kaon Photoproduction and the  $\Lambda$  Decay Parameter  $\alpha_-$ . *Phys. Rev. Lett.* 2019; **123**: 182301.
- [124] Dai LY, Haidenbauer J and Meißner UG. Re-examining the  $X(4630)$  resonance in the reaction  $e^+e^- \rightarrow \Lambda_c^+\bar{\Lambda}_c^-$ . *Phys. Rev. D* 2017; **96**: 116001.